ISSN 0912-232X

PHOTOMEDICINE AND PHOTOBIOLOGY

Vol.40 2018

The Japanese Society for Photomedicine and Photobiology

Photomedicine and Photobiology
Vol.40

2018

The Japanese Society for Photomedicine and Photobiology
Foundednin 1978

Office : Depaetment of Dermatology, Kobe University Graduate School of Medicine,
7-5-1 Kusunoki-cho, Chuo-ku, Kobe, 650-0017, Japan.

CONTENTS

Chemical and photobiological study of the structures and functions of DNA

Hiroshi Sugiyama[1,2]

[1]*Department of Chemistry, Graduate School of Science, Kyoto University, Kitashirakawa-Oiwakecho, Sakyo-ku, Kyoto 606-8502, Japan*
[2]*Institute for Integrated Cell-Material Sciences (WPI-iCeMS), Kyoto University, Yoshida-Ushinomiyacho, Sakyo-ku, Kyoto 606-8501, Japan*

Key words: DNA frame, 5-bromouracil, Pax6, Sox2, photoreaction

Abstract

This review describes the recent progress in our chemical and photobiological studies of the structures and functions of DNA. We used the DNA origami method to construct a new nanostructure, i.e., a "DNA frame." We used this nanoscale platform to successfully visualize the cooperative binding between Sox2 (Sex determining region Y-box 2) and Pax6 (Paired box protein) using high-speed atomic force microscopy. We demonstrated the cooperative binding of these transcription factors via photosensitization of 5-bromouracil-containing DNA by electron transfer from the tryptophan residues of the proteins. Our group also developed artificial genetic switches that switch the expression of selected genes on and off based on knowledge of chemical synthesis and molecular biology. We conjugated a histone deacetylase inhibitor to the *N*-methylpyrrole-*N*-methylimidazole polyamide, which recognizes the DNA sequence, to construct the ON switch. We demonstrated that one of the conjugates, SAHA (Suberoylanilide hydroxamic acid)-X, successfully upregulated retina-related genes, such as *Pax6*. We also established a new thG-tC (2-Aminothieno[3,4-d]pyrimidine G-mimic-tricyclic cytosine) FRET base pair system with replaceable native nucleobases that is fixed by base stacking and hydrogen bonding. We recorded distance- and orientation-dependent FRET after the formation of mononucleosome structures.

Introduction

Design of a DNA frame using the DNA origami method and visualization of enzymatic action

The DNA origami method was developed in 2006 by Rothemund and can be used to design and create a two-dimensional DNA structure with a size of ~100 nm.[1] In this method, a closed circular single-stranded DNA called m13 DNA and about 200 different short complementary DNA oligomers (mainly 32-mers) are used. After the annealing of these DNAs, self-assembled DNA origami structures can be obtained routinely. Using the DNA origami method, various 2D- and 3D-designed DNA nanostructures can be constructed. We created a 2D DNA structure called DNA frame to allow the direct observation of the behavior of DNA-modifying enzymes with double-stranded DNAs in an internal space of 40 ′ 40 nm.[2] We introduced 64 bp and 74 bp DNA bridges into the DNA frame, which provided tensed and relaxed duplexes, respectively. Using AFM, we visualized DNA-modifying enzymes directly on the DNA. We observed that a methylation enzyme was bound to DNA as a substrate. In addition, when the amount of methylation was estimated via a biochemical method, methylation occurred preferentially on the 74 bp vs the 64 bp DNA bridge (a threefold difference). Various DNA-modifying enzymes were investigated using this DNA frame system. We observed that a thymine dimer produced by irradiation with UVB was inserted into double-stranded DNA and a repair reaction by T4 pyrimidine dimer glycosylase was visualized.[3] The DNA recombination reaction is important for the generation of new genome sequences and for repairing damaged DNA. Therefore, the substrate DNA fragment was introduced into the DNA frame structure and the recombination reaction by Cre recombinase was examined. We visualized the recombination of the DNA chain through Holliday junction intermediate (two duplex cross-shaped DNA structure that forms during the process of genetic recombination) and the dissociation of Cre from the complex formed by Cre and the DNA chain using high-speed AFM. In this case, we were able to analyze the reaction by changing the orientation of the DNA strand using the DNA frame. We published these results as a review of three articles.[4–6] We recently used the DNA frame for visualizing the MOC1 protein, which is important for the segregation of chloroplasts.[7] We demonstrated that MOC1 effectively resolved a Holliday junction substrate.

Visualization of the cooperative binding of Sox2 and Pax6 and confirmation by photoreaction using ^{Br}U-substituted DNA

The selective regulation of gene expression has been achieved by pairing various transcription factors, followed by cooperative binding to the promoter region of genes. For example, Sox2 works with different transcription factors at different stages of development. In embryonic hepatocytes, Sox2 binds to Oct4 and maintains pluripotency. Sox2 also forms a pair with Pax6 to control the differentiation of cells into the nervous system, which is particularly important for eye differentiation. Therefore, the direct visualization of the binding of Sox2 and Pax6 to DNA was achieved using the DNA frame.[8] The results of

AFM imaging are shown in Figure 1. It was demonstrated that Sox 2 alone bound to the DNA bridge in the DNA frame and that it bound preferentially to the longer DNA bridge. However, under this condition, Pax6 alone did not bind to the DNA bridge, whereas it bound to the DNA bridge as a heterodimer in the presence of Sox2.

For many years, we investigated whether the photoreactivity of 5-halouracil could be used to probe the DNA local conformation and monitor the binding of small molecules and proteins. 5-Halo-2'-deoxyuridine is readily incorporated into DNA, and 5-halouracil-substituted DNA remains functional in vivo. However, the incorporation of 5-halouracil enhances the photosensitivity of cells with respect to DNA–protein crosslinking and DNA strand cleavage. We demonstrated that hydrogen abstraction by the uracil radicals that are generated in DNA duplexes strongly reflects the DNA local conformations.[9] Our laboratory has also developed a method to investigate the sequence-specific binding of proteins and small molecules to DNA using ^{Br}U-substituted DNA under 302 nm irradiation conditions. This method is based on the principle that electron transfer occurs from photoexcited tryptophan when the tryptophan residues of proteins are located near the ^{Br}U residues of DNA. The formation of a uracil radical after the elimination of the bromide ion produces a uracil residue in the presence of an excess amount of the hydrogen donor, which can be cleaved by uracil glycosidase treatment and subsequent heating conditions. Therefore, the occurrence of DNA cleavage indicates that the protein is bound in the vicinity of the DNA molecule. Fortunately, as tryptophan residues are present near the Sox2- and Pax6-binding sites, cooperative binding between these transcription factors was examined using ^{Br}U-substituted DNA under 302 nm irradiation conditions. It was revealed that Sox2 alone can bind to, and cleave DNA, whereas Pax6 cannot bind to DNA alone (Figure 2c). However, DNA cleavage by binding of Pax6 was observed in the presence of Sox2, and Pax6 was capable of binding to DNA only when Sox2 was present, indicating the cooperative binding of these proteins.[8]

Artificial genetic switches

Sequence-specific binding of the PIP

PIP is a modified peptide in which units of *N*-methylpyrrole (P) and *N*-methylimidazole (I) are linked by a peptide bond. The incorporation of aminobutyric acid leads to the folding of the PI polyamide into a hairpin shape and to its binding to double-stranded DNA in a sequence-specific manner with the same strength as that observed for the transcription factor.[11] The sequence specificity follows a simple recognition rule: i.e., the pair of I and P recognizes GC base pairs, and the pair of P and P recognizes AT base pairs or TA base pairs. Therefore, by changing the sequence of P and I, it is possible to design a PIP that binds to specific DNA sequences. For this reason,

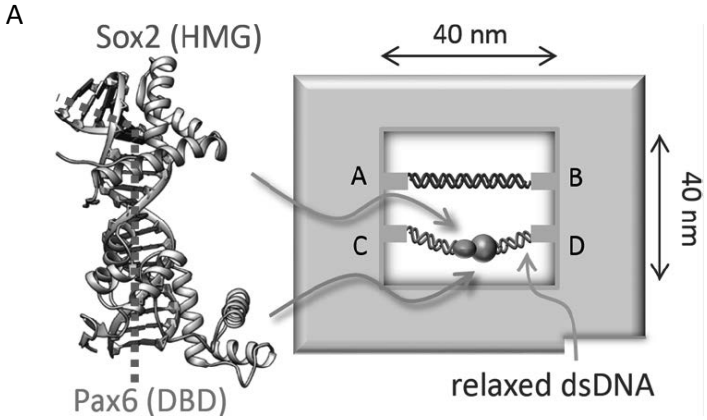

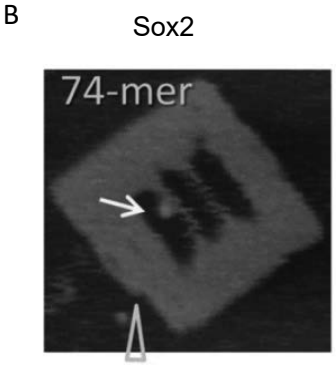

C

Protein Occupancy (%) on Various DNA Bridges

	Sox2	Pax6	Sox2-Pax6
64-mer DNA	2.5	0	3.6
69-mer DNA	3.7	0	4.6
74-mer DNA	4.7	0	9.8

Figure 1. Direct observation of the cooperative binding of the transcription factors Sox2 and Pax6 in the DNA frame. (A) The model structure of the Sox2/Pax6 complex on the putative DNA element and DNA frame with a vacant area inside containing four connection sites: A, B, C, and D. The two DNA strands of the 64-mer and 74-mer DNA bridges. (B) Representative AFM image of Sox2 and Sox2/Pax6 bound to a 74-mer dsDNA. (C) Quantification of protein occupancy on various DNA bridges.

it is possible that PIP can deliver various functional molecules to a specific sequence in the genome.

A functional Py-Im polyamide that distinguishes telomeric sequences

As described above, because PIP binds to the minor groove of double-stranded DNA in a sequence-specific manner, a fluorescent PIP that binds specifically to a telomeric region located at the end of a chromosome was synthesized. To improve the specificity of PIP for the human telomeric sequence (5'–TTAGGG–3'/5'–CCCTAA–3')$_n$, we developed a novel synthetic method of connecting the hairpin PIP to synthesize a tandem dimer, trimer, and tetramer.[12–14] These structures can be used as tools for telomere research because the fluorescent PIP binds to DNA without melting of the double-stranded DNA. We visualized specific fluorescence from the telomeric region in human HeLa cells and mouse MC12 cells with a long telomere under mild conditions. We also examined the possibility of cancer diagnosis using telomere-specific imaging. We estimated the length of telomeres and cleared the path for the clinical application of the sequence-specific binding of PIP.[15] We demonstrated further that the specificity of PIP for the telomere is increased by expanding the molecule from a tandem dimer to a tandem trimer, and then to a tandem tetramer. Moreover, using a biotinylated tandem tetramer, we demonstrated that this molecule selectively binds to the telomeric region of human chromosomes, as revealed by pull-down experiments and a subsequent next-generation sequencing (NGS) analysis.[16] As this polyamide can bind to double-stranded DNA, visualization under milder conditions becomes possible. We have not succeeded in performing live-cell imaging, because the molecule becomes large and it is poorly incorporated into the nucleus. It is expected that further improvement of molecular structures and conditions will allow live-cell imaging.

Design of the PIP OFF switch

As PIP has excellent sequence-specific DNA-binding properties and excellent accumulation in the nucleus, it is one of the promising building blocks of artificial genetic switches. Because binding to DNA is similar to that of transcription factors, it is possible to inhibit the binding of transcription factors, and the suppression of the expression of various genes in this manner has been reported. In addition, even in coding regions, gene expression can be suppressed by alkylation of the template strand in a sequence-specific manner. First, we attempted to suppress the expression of oncogenes via the conjugation of an alkylating agent to PIP. It has been shown that mutations of *KRAS* occur frequently in colon cancer and pancreatic cancer. Among them, the mutation from GGT to GTT at codon 12 is well known. Therefore, we synthesized KR12, to react with the complementary strand of this mutated GTT sequence.[17] This molecule selectively reacted with the mutated sequence of *KRAS* and selectively inhibited KRAS expression. The injection of KR12 into a mouse bearing human colon cancer via the tail vein led to the obvious suppression of the growth of the cancer, and it was revealed that the bulging of the cancer tissue had disappeared almost completely 5 weeks after the injection. These results indicate that the DNA base sequence is sufficient as a molecular target for cancer treatment and is expected to be a new tailor-made anticancer drug.

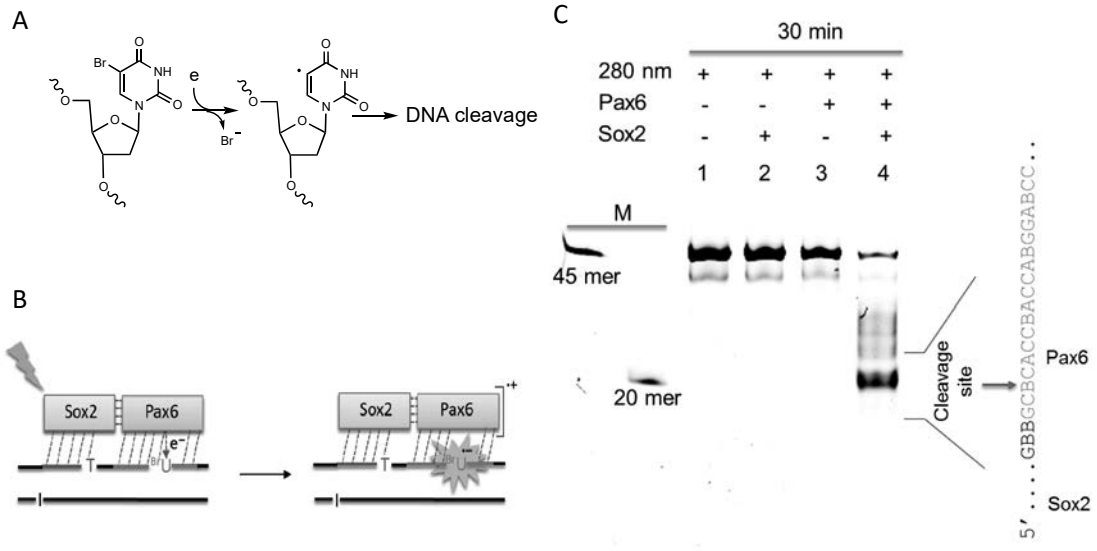

Figure 2. The detection of cooperative binding of the transcription factors Sox2 and Pax6 by photoreaction of ^{Br}U-substituted DNA. (A) The formation of a uracil radical by electron transfer induced DNA cleavage. (B) Upon photoirradiation of the Sox2–Pax6–DNA complex, an electron is injected from Pax6 to the ^{Br}U residue. (C) Pax 6 itself did not induce cleavage of ^{Br}U-substituted DNA, but ^{Br}U-substituted DNA was cleaved when Sox 2 was present. The ^{Br}U residue at the binding site of Sox 2 was converted with T.

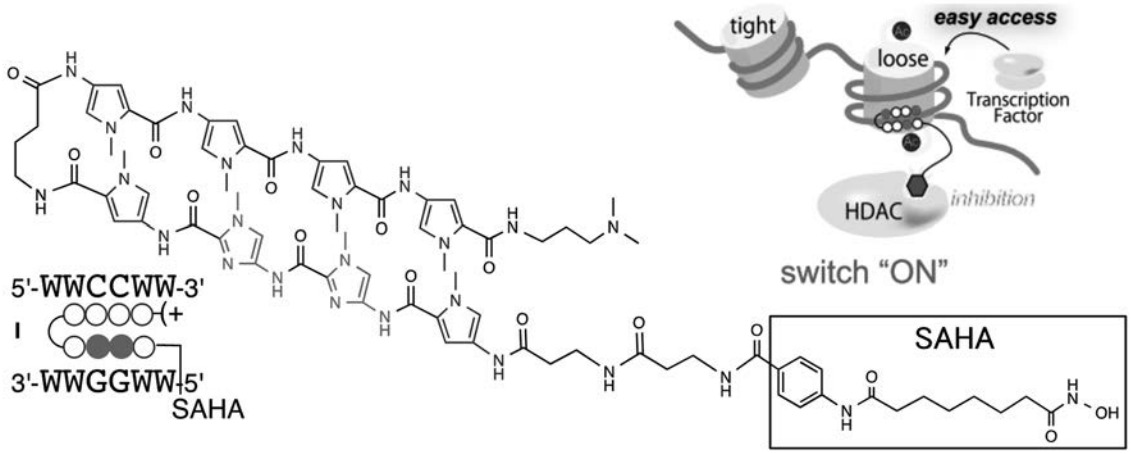

Figure 3. Histone is acetylated by HDAC inhibition, the nucleosome structure becomes loose, the transcription factor binds to the molecule, and the expression of the gene is turned ON.

Design of ON switch

It has become clear that gene expression is controlled by DNA sequence information, as well as by epigenetic modifications, such as histone acetylation and methylation, and DNA methylation. To activate the expression of specific genes, it is necessary to consider epigenetic changes, such as histone acetylation. Therefore, SAHA, which is an HDAC inhibitor, was conjugated to PIP, and we tried to activate selective gene activation using this conjugate (Figure 3).[18]

Because selective gene activation did not yield clear results in terms of the sequence specificity of PIP, 32 types of SAHA–PIP libraries that were expected to bind to different base sequences were synthesized, and gene activation was investigated using human skin fibroblasts (HDFs). The results of a microarray assay after treatment of HDFs with 1 mM SAHA–PIP for 48 h revealed that most of the SAHA–PIP molecules activated the expression of 200 genes by >10-fold under these conditions. We showed that most of the activated genes are unique genes and proved our hypothesis that SAHA–PIP activates genes in a sequence-specific fashion. In addition, we confirmed that SAHA–PIP-E, -F, -H, and -I increased the expression of pluripotency-related genes, such as *Sox2* and *Nanog*. As shown in Figure 4, SAHA–PIP-X in the library activated retina-related gene groups, such as *Pax6*, *RS1*, *USH2A*, *CRYBB3*, and *STRA6*.[19] Using the biotinylated SAHA–PIP-X, we demonstrated that the binding site on the genome selectively bound to the encoded portion of PAX6 and the promoter region, as examined by NGS analysis. These results suggest that SAHA–PIP can be used for the treatment of diseases that are caused by repression of gene

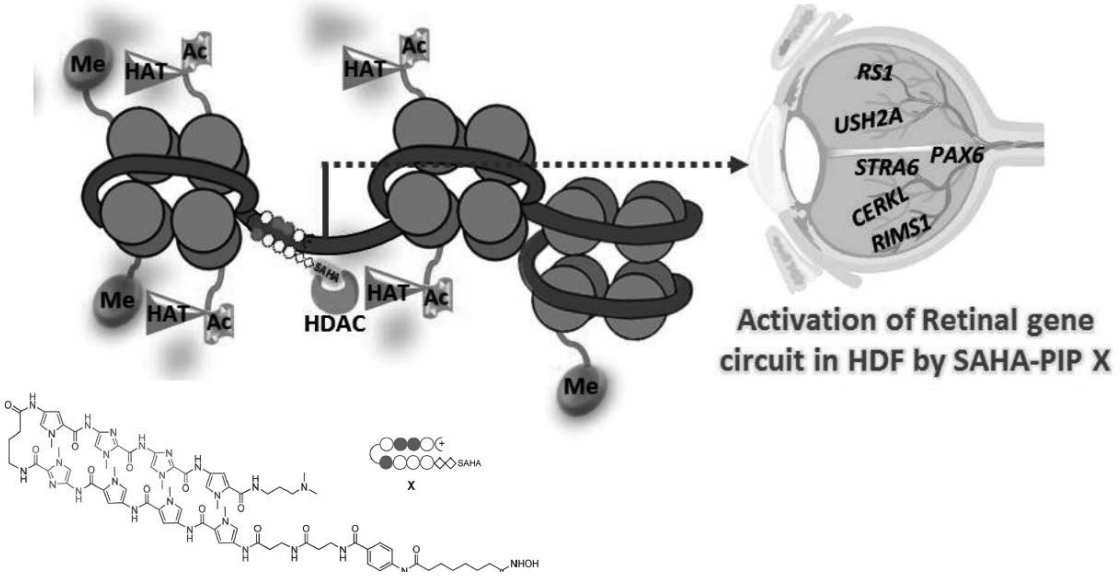

Figure 4. HDFs were specifically inhibited by DNA base sequence by AHA–PIP-X, and activation of retina-related gene groups, such as *Pax6*, *RS1*, *USH2A*, *CRYBB3*, and *STRA6*, occurred.

expression.

New FRET system for nucleosomes

We are also interested in the dynamic structure of nucleosomes because gene expression involves chromatin structure. Förster Resonance Energy Transfer (FRET) has been used for the analysis of the dynamic structural changes of nucleosomes. In conventional systems, however, dyes attach to DNA bases or histone proteins with a flexible carbon linker. Moreover, these dyes can be randomly rotated; thus, it is difficult to discuss the accurate dynamics of nucleosomes. Therefore, we introduced thdG as a donor and tC as an acceptor with base pairing with normal G and C in our new FRET system. To examine the new FRET system, we prepared 31-mer oligonucleotides containing thdG or tC at different positions and assessed the distance dependency between the donor and the acceptor.[20]

Based on these observations, we prepared three PCR primers containing thdG or tC and amplified 601 nucleosome positioning sequences.[21] After PCR amplification, we reconstituted the nucleosome using a salt dialysis method. The steady-state fluorescence of mononucleosomes is shown in Figure 5B. The dashed line indicates nucleosomes containing only a donor, and the solid line shows nucleosomes containing a donor and an acceptor. As compared with nucleosome with D 40th + A 41st, higher quenched donor emission of nucleosome with D 40th + 27th was obtained around 450 nm. Furthermore, nucleosomes with D 40th + A 27th exhibited a longer emission maximum (471 nm) than did nucleosomes with D 40th + A 41st, suggesting that the former have a higher FRET efficiency than the latter (469 nm). After deconvolution, FRET efficiencies were calculated as shown in Figure 5C. The present FRET system can provide a deeper insight into the conformational changes of DNA on nucleosomes in the presence of our artificial genetic switch, as well as promote the understanding of the mechanism of intrinsic genetic processes.

Conclusions

We developed a new DNA frame using the DNA origami method and demonstrated that the retina-related Pax6 and Sox2 cooperatively bind to the target sequence. Using a photo reaction of ^{Br}U-containing DNA, we also obtained evidence of the cooperative binding of these transcription factors. Moreover, we developed SAHA–PIP-X to upregulate retina-related genes. Various diseases have been associated with epigenetic changes. Understanding the mechanism of control of gene expression at the molecular level would lead to novel diagnoses of diseases and even to rational therapies. Genetic switches that possibly serve as tools that regulate the expression of specific gene could be used for the treatment of various diseases. We applied a highly emissive nucleobase thdG-tC FRET system to 601 nucleosomes for the first time. The nucleosomal DNA containing the thdG-tC FRET pair was successfully amplified by PCR, and its DNA wrapped around nucleosomes, similar to that observed in the natural condition. We calculated the FRET efficiencies and orientation factors of two nucleosomes by changing the location of the acceptors. We hope to be able to control gene expression and create innovative treatments by further combining the tools of chemical biology introduced in this article.

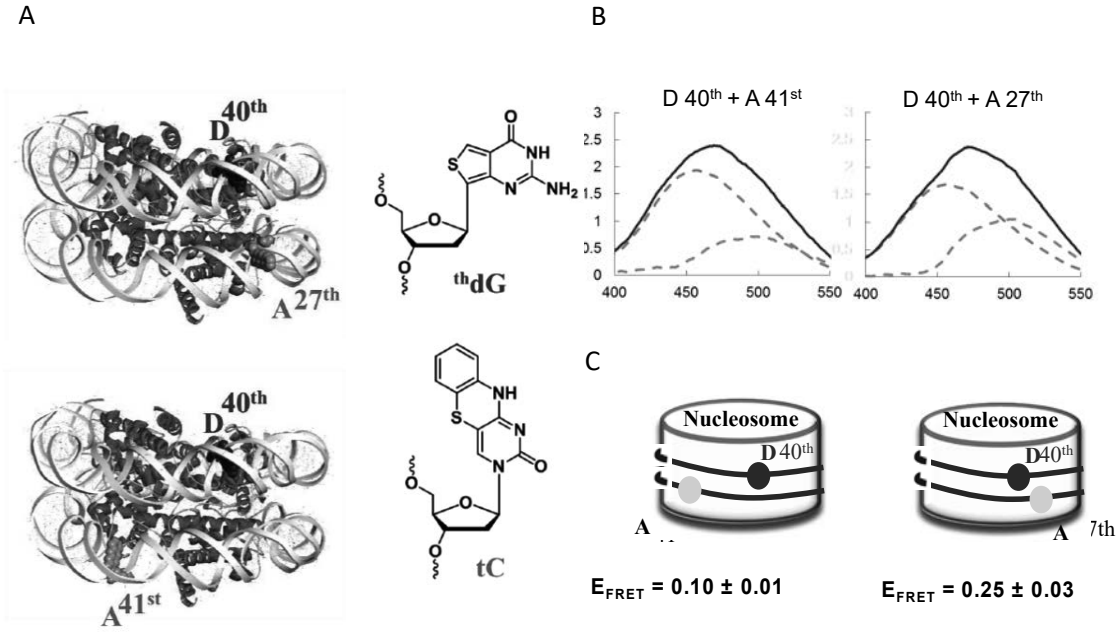

Figure 5. thG-tC FRET system of nucleosomal DNA. (A) Schematic presentation of 601 145 bp sequences containing a donor, thG (40th), and an acceptor, tC (27th and 41st). (B) Fluorescence emission spectra of a nucleosome containing a donor (D 40th) and an acceptor (27th and 41st), and deconvoluted emission spectra. (C) Calculated FRET efficiencies of two nucleosomes (D 40th + A 41st or 17 D 40th + A 27th), with mean errors.

Acknowledgments

This work was supported by a Grant-in-Aid for Scientific Research form the Ministry of Education, Culture, Sports, Science and Technology (MEXT) of the Japanese Government.

References

1. Rothemund PW: Folding DNA to Create Nanoscale Shapes and Patterns. Nature, 2006; **440**: 297-302.
2. Endo M, Katsuda Y, Hidaka K et al: Regulation of DNA Methylation Using Different Tensions of Double Strands Constructed in a Defined DNA Nanostructure. *J. Am. Chem. Soc.,* 2010; **132**: 1592-1597.
3. Kobayashi Y, Misumi O, Odahara M et al: Holiday Junction Resolvases Mediate Chlorophast Nucleoid Segregation. Science, 2017; **356**: 631-634.
4. Pandian G N, Sugiyama H: Nature-Inspired Design of Smart Biomaterials Using the Chemical Biology of Nucleic Acids. *Bull. Chem. Soc. Jpn.,* 2016; **89**: 843-868.
5. Endo M, Sugiyama H: Single-Molecule Imaging of Dynamic Motions of Biomolecules in DNA Origami Nanostructures Using High-Speed Atomic Force Microscopy. *Acc. Chem. Res.,* 2014; **47**: 1645-1653.
6. Rajendran A, Endo M, Sugiyama H: State-of-the-Art High-Speed Atomic Force Microscopy for Investigation of Single-Molecular Dynamics of Proteins. *Chem. Rev.,* 2014; **114**: 1493-1520.
7. Endo M, Katsuda Y, Hidaka K et al: A Versatile DNA Nanochip for Direct Analysis of DNA Base-Excision Repair. *Angew. Chem. Int. Ed.,* 2010; **49**: 9412-9416.
8. Yamamoto S, De D, Hidaka K, Kim K K et al: Single Molecule Visualization and Characterization of Sox2-Pax6 Complex Formation on a Regulatory DNA Element Using a DNA Origami Frame. *Nano Lett.,* 2014; **14**: 2286-2292.
9. Xu Y, Tashiro R, Sugiyama H: Photochemical Determination of Different DNA Structures. *Nature Protocols* 2007; **2**: 78-87.
10. Saha A, Kizaki S, De D et al: Examining Cooperative Binding of Sox2 on DC5 Regulatory Element upon Complex Formation with Pax6 through Excess Electron Transfer Assay. *Nucleic Acids Res.,* 2016; **44**: e125.
11. Gottesfeld JM, Neely L, Trauger JW, et al: Regulation of Gene Expression by Small Molecules. *Nature*, 1997; **387**: 202-205.
12. Kawamoto Y, Bando T, Kamada F, et al: Development of a New Method for Synthesis of Tandem Hairpin Pyrrole-Imidazole Polyamide Probes Targeting Human Telomeres. *J. Am. Chem. Soc.,* 2013; **135**: 16468-16477.
13. Hirata A, Nokihara K, Kawamoto Y et al: Structural Evaluation of Tandem Hairpin Pyrrole-Imidazole Polyamides Recognizing Human Telomeres. *J. Am. Chem. Soc.,* 2014; **136**: 11546-11554.
14. Kawamoto Y, Sasaki A, Hashiya K et al: Tandem Trimer Pyrrole-Imidazole Polyamide Probes Targeting 18 Base Pairs in Human Telomere Sequences. *Chem. Sci*., 2015; **6**: 2307-2312.
15. Sasaki A, Ide S, Kawamoto Y et al: Telomere Visualization in Tissue Sections using Pyrrole-Imidazole Polyamide Probes *Sci. Rep.,* 2016; **6**: 29261.
16. Kawamoto Y, Sasaki A, Chandran A et al: Targeting 24 bp withn Telomere Repeat Sequences with Tandem Tetramer Pyrrole-Imidazole Polyamide Probes. *J. Am. Chem. Soc.,* 2016; **138**: 14100-14107.
17. Hiraoka K, Inoue T, Taylor R D et al: Inhibition of KRAS Codon 12 Mutants Using a Novel DNA-Alkylating Pyrrole-Imidazole Polyamide Conjugate. *Nature Commun.,* 2015; **6**: 6706.
18. Pandian G N, Taniguchi J, Junetha S et al: Distinct DNA-Based Epigenetic Switches Trigger Transcriptional Activation of Silent Genes in Human Dermal Fibroblasts. *Sci. Rep.,* 2014; **4**: 3843.
19. Syed J, Chandran A, Pandian G N et al: A Synthetic Transcriptional Activator of Genes Associated with the Retina in Human Dermal Fibroblasts. *ChemBioChem,* 2015; **16**: 1497-1501.
20. Han J, Yamamoto S, Park S, Sugiyama H: Development of a Vivid FRET System Based on a Highly Emissive dG-dC Analogue Pair *Chem. Eur. J.,* 2017; **23**: 7607-7613.
21. Han J, Park S, Hashiya F, Sugiyama H: Novel Approach to the Investigation of Nucleosome Structure Using the Highly Emissive Nucleobase thdG-tC FRET Pair. *Chem. Eur. J.,* 2018; **24**: 17091-17095.

Photosensitizing Activity of Berberine-Cyclodextrin Inclusion Complexes

Kazutaka Hirakawa[1,2,*], Akiko Kitagawa[1], Shigetoshi Okazaki[3], Fumitoshi Ema[4], and Yasuhiro Kobori[4,5]

[1] *Applied Chemistry and Biochemical Engineering Course, Department of Engineering, Graduate School of Integrated Science and Technology, Shizuoka University, Johoku 3-5-1, Naka-ku, Hamamatsu, Shizuoka 432-8561, Japan*

[2] *Department of Optoelectronics and Nanostructure Science, Graduate School of Science and Technology, Shizuoka University, Johoku 3-5-1, Naka-ku, Hamamatsu, Shizuoka 432-8561, Japan*

[3] *Preeminent Medical Photonics Education & Research Center, Hamamatsu University School of Medicine, Handayama 1-20-1, Higashi-ku, Hamamatsu, Shizuoka 431-3192, Japan*

[4] *Department of Chemistry, Graduate School of Science, Kobe University, 1-1 Rokkodai, Nada-ku, Kobe 657-8501, Japan*

[5] *Laser MolecularPhotoscience Laboratory, Molecular Photoscience Research Center, Kobe University, 1-1 Rokkodai, Nada-ku, Kobe 657-8501, Japan*

Abstract: Berberine, an alkaloid, forms inclusion complex with α- and β-cyclodextrins through an entropy effect. The photoexcited state of berberine is rapidly quenched in an aqueous solution, however the lifetime of singlet excited state of berberine was markedly elongated in the hydrophobic cavity of cyclodextrin. Furthermore, the intersystem crossing to triplet excited state of berberine was enhanced by this interaction. Singlet oxygen generation of berberine was not increased by cyclodextrin, possibly due to the inhibition of the interaction between berberine in the cyclodextrin cavity and oxygen molecule.

Keywords: Berberine, Cyclodextrin, Photosensitizer, Triplet excited state, Singlet oxygen

INTRODUCTION

Berberine (5,6-dihydro-9,10-dimethoxybenzo[g]-1,3-benzodioxolo[5,6-a]quinolizinium; BBR) is an alkaloid isolated from Goldenseal (*Hydrastis canadensis* L.) [1]. Its antibacterial and anti-inflammatory effects have been reported, and it is marketed as an antidiarrheal [2,3]. Furthermore, BBR does not show toxicity under dark condition [2,3]. We have previously reported that the photoexcited state of BBR is rapidly quenched through intramolecular electron transfer and an electrostatic interaction with DNA suppresses this quenching, resulting in the enhancement of fluorescence emission and singlet oxygen ($^1O_2$) generation [4,5]. This characteristic might be applied to photodynamic therapy (PDT), a promising less invasive cancer therapy using a non-thermal visible light [6], through DNA-selective mechanism as a target biomolecule [7]. Cyclodextrin (CD), which is a non-toxic cyclic glucose, can be employed in supramolecular medicine [8]. CDs form an inclusion complexes with BBR using its hydrophobic cavity [9-11]. Relevantly, more complex supramolecular system including a CD derivative and BBR was reported [12]. However, the photochemical property of inclusion complex of CDs and BBR has not been well understood. In general, a hydrophobic environment inhibits photoinduced electron transfer [13-15], because of a stabilization of the energy level of charge transfer state [16]. It is speculated that the intramolecular electron transfer-mediated quenching of photoexcited state of BBR is suppressed in the hydrophobic cavity of CDs, resulting in the enhancement of the intersystem crossing to the triplet excited (T_1) state and energy transfer to oxygen molecule. Therefore, the interaction with CD may use to control the PDT activity of BBR. In this study, the association between BBR and CD (α-, β-, and γ-CD) (Fig. 1) and the photochemical properties of these inclusion complexes were investigated.

EXPERIMENTAL

BBR (or palmatine, an analogue of BBR) chloride (Wako Pure Chemical Industries, Ltd., Tokyo Japan) was mixed with CD in a 10 mM sodium phosphate buffer (pH 7.6) to measure absorption and fluorescence spectra. This experimental condition at pH 7.6 was selected as a

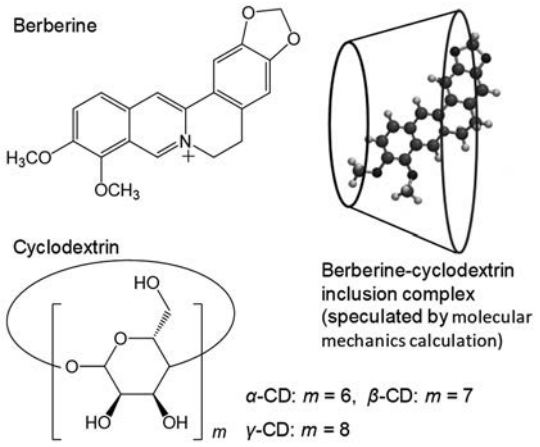

Fig. 1 Structures of berberine, cyclodextrin, and image of the inclusion complex.

physiological condition model. Indeed, photosensitized DNA damage by various drugs has been examined at around this pH condition [17-19]. In addition, the interaction between BBR and DNA was examined at this pH [4,5]. Fluorescence lifetime (τ_f) and transient absorption spectra of this sample solutions were also measured [20]. Time-resolved electron paramagnetic resonance (EPR) measurement was performed to examine the T_1 state of BBR with CD [21]. The $^1O_2$ generation was directly measured by near-infrared luminescence at around 1270 nm from $^1O_2$, which corresponds to the $^1O_2(^1\Delta_g)$–$^3O_2(^3\Sigma_g^-)$ transition [4,22].

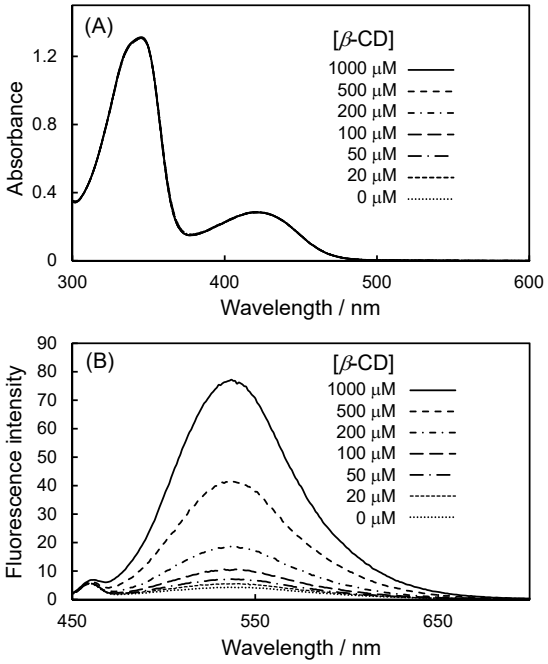

Fig. 2 Absorption spectra of BBR with β-CD (A) and their fluorescence spectra (B). The sample solution contained 50 μM BBR and the indicated concentration of β-CD in a 10 mM sodium phosphate buffer (pH 7.6). The excitation wavelength was 400 nm.

RESULTS AND DISCUSSION

Absorption and fluorescence spectra of BBR with or without β-CD are shown in Fig. 2. Similar results were observed in the cases of α-CD. Absorption spectrum of BBR was barely changed by the addition of CDs (Fig. 2A). Therefore, the analysis of interaction between BBR and CDs was difficult by absorption spectrum measurement. Fluorescence intensity of BBR is very small by the rapid deactivation process in aqueous solution [4,5]. In the presence of α- or β-CD, the fluorescence intensity (Fig. 2B) and τ_f (described in later) of BBR markedly increased, suggesting the formation of inclusion complex (BBR-CD_n) as follows:

$$BBR + nCD \rightleftarrows BBR\text{-}CD_n \qquad (1).$$

Table 1 Association constant and thermodynamic parameter of the inclusion complex of berberine and α- and β-CD

	K	ΔH^o	ΔS^o	ΔG^o
	M^{-1}	kJ mol^{-1}	J K^{-1}	kJ mol^{-1}
α-CD	3,500	8.8	59	-8.8
β-CD	7,500	1.4	37	-9.6

These parameters were determined using 50 μM BBR and 0-200 μM α- or β-CD in a 10 mM sodium phosphate buffet (pH 7.6) at 298 K.

Interestingly, γ-CD did not show the fluorescence enhancement effect of BBR. In addition, the fluorescence spectrum of palmatine, an analogue of BBR, was not changed by the addition of these CDs in this experimental condition. These results suggest that γ-CD is too large to form a stable complex with BBR and the slight bulky strucuture of palmatine compared with BBR is not appropriate for the interaction with CDs. Molecular mechanics calculation also supports the stable inclusion complex formation between BBR and α- and β-CD (Fig. 1). From the analysis of the fluorescence intensity of BBR with CD, the association constant (K) was calculated using the following equations:

$$K = \frac{[\mathrm{BBR{-}CD}_n]}{[\mathrm{BBR}][\mathrm{CD}]^n} \qquad (2)$$

and

$$Log\frac{F_0 - F}{F} = Log\,K + n Log[\mathrm{CD}] \qquad (3)$$

where [BBR], [CD], and [BBR-CD_n] are the concentrations of BBR, CD, and the inclusion complex, respectively, F_0 is the fluorescence intensity of BBR without CD, and F is that with CD. In the case of relatively low concentration of CD (the concetration ratio of BBR and CD is around 1:1), the n became unity, suggesting the formation of 1:1 complex. In the presence of excess amount of CD, the n became 0.4 (α-CD) and 0.2 (β-CD), suggesting the aggregation of CD molecules around the 1:1 BBR-CD complex. The thermodynamic parameters of this 1:1 inclusion complexation at standard state, enthalpy change (ΔH^o), entropy change (ΔS^o), and Gibbs energy (ΔG^o), were calculated from the temperature dependence of K values by van't Hoff equation (Table 1). Obtained ΔH^o and ΔS^o values were positive. These analyzed values indicate that the entropy effect is a driving force of this interaction. This interaction mechanism at pH 7.6 is different from the reported interaction between β-CD and BBR under basic condition [10]. In addition, these results suggest that this complexation between these CDs and BBR proceeds through a hydrophobic interaction under this experimental condition [23].

The fluorescence enhancement of BBR through inclusion complexation can be explained by the inhibition of intra-molecular electron trasfer [4,5] in a hydrophobic cavity of CD. Fluorescence lifetime measurement showed

that the singlet excited (S_1) state lifetime of BBR in sodium phosphate buffer (τ_f = 0.12 ns; without CD) is markedly elongated in the complex form with CD (τ_f = 1.9 ns; α-CD and 3.0 ns; β-CD). These τ_f values were shorter than those of BBR with DNA, suggesting that the electron transfer-mediated quenching is not completely inhibitted by CDs.

It was reported that photoexcited BBR in an aqueous solution does not produce the T_1 state due to rapid non-radiative quenching [24]. However, in the presence of DNA, the S_1 state lifetime increases and the intersystem crossing to the T_1 state is enhanced [4,5,7]. Therefore, the T_1 state formation of BBR with β-CD, of which the K value with BBR is larger than that of α-CD, was examined. Time resolved EPR measurement demonstrated the formation of BBR T_1 state in the presence of β-CD (Fig. 3). The time profile of this signal could be fitted by double exponential function and the analyzed lifetimes (1.2 μs; 48% and 16 μs; 52%) were comparable with those of BBR-DNA complex in an aqueous solution [4]. Furthermore, a transient absorption spectrum around 400-700 nm, which is assigned to BBR T_1 state by the theoretical calculation of the density functional treatment at the B3LYP/6-31G* level, was obseved and the intensity was increased by the addition of β-CD. These findings indicated that photoexcited BBR can produce its T_1 state in the CD cavity.

Photosensitized $^1O_2$ generation by BBR was examined by a near-infrared emission measurement. The quantum yield of $^1O_2$ generation (Φ_Δ) was estimated from the comparison of the emission intensity with that of methylene blue (Φ_Δ = 0.52 in water) [25]. The $^1O_2$ generation by

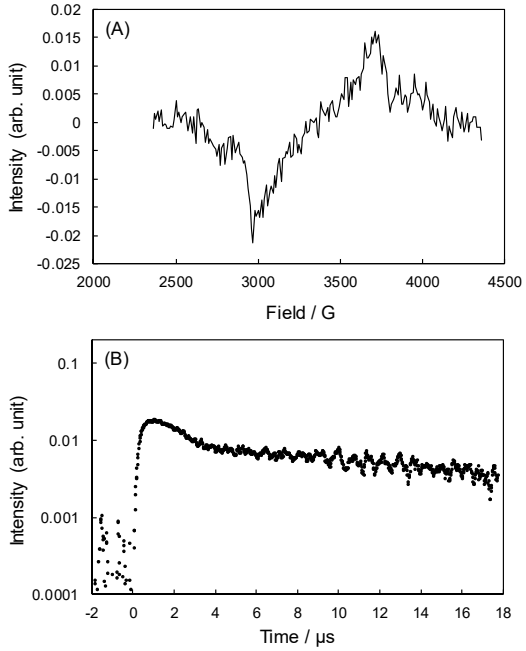

Fig. 3 Time resolved EPR spectrum of BBR obtained 0.7 μs after 355 nm laser excitation at 77 K (A) and the time profile of the absolute value of signal at 3000 G (B). The sample solution contained 50 μM BBR and 200 μM β-CD in a 10 mM sodium phosphate buffer (pH 7.6) with ethylene glycol.

BBR in ethanol was confirmed (Φ_Δ=0.072), however, the estimated value in water was very small (0.018). In the presence of CD, the $^1O_2$ generation activity of BBR was barely increased. These results can be explained by that the inclusion complexation with CD inhibits the interaction including energy transfer from the T_1 state of BBR to oxygen molecule [26].

CONCLUSIONS

BBR forms an inclusion complex with α- and β-CDs through entropy effect. Specifically, more stable complex is formed with β-CD. The S_1 state lifetime of BBR is markedly elongated and the T_1 state formation is enhanced through this inclusion complexation. However, $^1O_2$ generation activity of BBR is not improved by CD, possibly due to the inhibition of the interaction with oxygen molecule. Therefore, α- or β-CD can be used as a carrier of BBR, and the dissociation from the inclusion complex by a controlled release technique [12] and an interaction with other biomolecules, *e.g.* DNA, is necessary for the photodynamic action of BBR.

Acknowledgments

This work was supported in part by Grant-in-Aid for Scientific Research (B) from Japanese Society for the Promotion of Science (JSPS KAKENHI 17H03086).

Notes

The authors declare no conflict of interests.

References

1. Weber HA, Zart MK, Hodges AE, Molloy HM, O'Brien BM, Moody LA, Clark AP, Harris RK, Overstreet JD, Smith CS. Chemical comparison of Goldenseal (*Hydrastis canadensis* L.) root powder from three commercial suppliers. J Agric Food Chem, 2003;51:7352–7358.
2. Neag MA, Mocan A, Echeverría J, Pop RM, Bocsan CI, Crişan G, Buzoianu AD. Berberine: botanical occurrence, traditional uses, extraction methods, and relevance in cardiovascular, metabolic, hepatic, and renal disorders. Front Pharmacol, 2018;21:557.
3. Chen CY, Kao CL, Liu CM. The cancer prevention, anti-inflammatory and anti-oxidation of bioactive phytochemicals targeting the TLR4 signaling pathway. Int J Mol Sci, 2018;19:2729.
4. Hirakawa K, Hirano T, Nishimura Y, Arai T, Nosaka Y. Dynamics of singlet oxygen generation by DNA-binding photosensitizers. J Phys Chem B, 2012;116:3037–3044.
5. Hirakawa K, Hirano T. The microenvironment of DNA switches the activity of singlet oxygen generation photosensitized by berberine and palmatine. Photochem Photobiol, 2008;84:202–208.
6. Dolmans DEJGJ, Fukumura D, Jain RK. Photodynamic therapy for cancer. Nat Rev Cancer, 2003;3:380–387.

7. Hirakawa K, Kawanishi S, Hirano T. The mechanism of guanine specific photooxidation in the presence of berberine and palmatine: activation of photosensitized singlet oxygen generation through DNA-binding interaction. Chem Res Toxicol, 2005;18:1545−1552.
8. Gangemi CMA, Puglisi R, Pappalardo A, Trusso Sfrazzetto G. Supramolecular complexes for nanomedicine. Bioorg Med Chem Lett, 2018;28:3290−3301.
9. Yang Y, Yang HF, Liu YL, Liu ZM, Shen GL, Yu RQ. Cetyltrimethylammonium assay using fluorescence probe berberine and a competitive host–guest complexation with butylated *β*-cyclodextrin. Sensors Actuators B, 2005;106: 632−640.
10. Jia B, Li Y, Wang D, Duan R. Study on the interaction of β-cyclodextrin and berberine hydrochloride and its analytical application. PLoS One, 2014;9:e95498.
11. He A, Kang X, Xu Y, Noda I, Ozaki Y, Wu J. Investigation on intermolecular interaction between berberine and *β*-cyclodextrin by 2D UV–Vis asynchronous spectra. Spectrochimica Acta A, 2017;185:343−348.
12. Chen XM, Chen Y, Hou XF, Wu X, Gu BH, Liu Y. Sulfonato-*β*-cyclodextrin mediated supramolecular nanoparticle for controlled release of berberine. ACS Appl Mater Interfaces, 2018;10:24987–24992.
13. Hirakawa K, Segawa H. Excitation energy transfer and photo-induced electron transfer in axial bispyrenyl phosphorus porphyrin derivatives: factors governing the competition between energy and electron transfer processes under the existence of intramolecular π-π interaction. J Photochem Photobiol A, 1999;123:67–76.
14. Hirakawa K, Saito K, Segawa H. Anomalously selective quenching of S_2 fluorescence from upper excited state of zinc 5-(1'-pyrenyl)-10,15,20-triphenylporphyrin derivatives through intramolecular charge transfer state. J Phys Chem A, 2009;113:8852–8856.
15. Horiuchi H, Kuribara R, Hirabara A, Okutsu T. pH-Response optimization of amino-substituted tetraphenylporphyrin derivatives as pH-activatable photosensitizers. J Phys Chem A, 2016;120:5554–5561.
16. Weller A. Photoinduced electron transfer in solution. Z Phys Chem Noue Folge, 1982;133:93–98.
17. Kawanishi S, Hiraku Y, Oikawa S. Mechanism of guanine-specific DNA damage by oxidative stress and its role in carcinogenesis and aging. Mutat Res., 2001;88:65–76.
18. Hirakawa K, Mori M, Yoshida M, Oikawa S, Kawanishi S. Photo-irradiated titanium dioxide catalyzes site specific DNA damage via generation of hydrogen peroxide. Free Radic Res, 2004;38:439–447.
19. Tada-Oikawa S, Oikawa S, Hirayama J, Hirakawa K, Kawanishi S. DNA damage and apoptosis induced by photosensitization of 5,10,15,20-tetrakis (*N*-methyl-4-pyridyl)-21*H*,23*H*-porphyrin via singlet oxygen generation. Photochem Photobiol, 2009;85:1391–1399.
20. Hirakawa K, Ito H. Rhodamine-6G can photosensitize folic acid decomposition through electron transfer. Chem Phys Lett, 2015;627:26–29.
21. Kobori Y, Ponomarenko N, Norris Jr. JR. Time-resolved electron paramagnetic resonance study on cofactor geometries and electronic couplings after primary charge separations in the photosynthetic reaction center. J Phys Chem C, 2015;119:8078–8088.
22. Hirakawa K, Ouyang D, Ibuki Y, Hirohara S, Okazaki S, Kono E, Kanayama N, Nakazaki J, Segawa H. Photosensitized protein-damaging activity, cytotoxicity, and antitumor effects of P(V)porphyrins using long-wavelength visible light through electron transfer. Chem Res Toxicol, 2018;31:371–379.
23. Moradi Z, Khorasani-Motlagh M, Rezvani AR, Noroozifar M. Electronic and fluorescent studies on the interaction of DNA and BSA with a new ternary praseodymium complex containing 2,9-dimethyl 1,10-phenanthroline and antibacterial activities testing. J Biomol Struct Dyn, 2019;37:2283–2295.
24. Inbaraj JJ, Kukielczak BM, Bilski P, Sandvik SL, Chignell CF. Photochemistry and photocytotoxicity of alkaloids from Goldenseal (*Hydrastis canadensis* L.) 1. Berberine. Chem Res Toxicol, 2001;14:1529–1534.
25. Usui Y, Kamogawa K. A standard system to determine the quantum yield of singlet oxygen formation in aqueous solution. Photochem Photobiol, 1974;19:245–247.
26. Lang K, Mosinger, J, Wagnerová DM. Photophysical properties of porphyrinoid sensitizers non-covalently bound to host molecules; models for photodynamic therapy. Coordination Chem Rev, 2004;248:321–350.

Glutathione arrest in the pores of mesoporous silica nanoparticles bearing maleimide units to enhance the radiation effects

Midori Ito, Ryohsuke Kurihara and Kazuhito Tanabe*

Department of Chemistry and Biological Science, College of Science and Engineering, Aoyama Gakuin University, 5-10-1 Fuchinobe, Chuo-ku, Sagamihara, Kanagawa 252-5258, Japan

ABSTRACT

Glutathione (GSH) is one of the main non-protein thiols present in cells, and it exhibited a protective effect in tumor radiation therapy. Therefore, the reduction of GSH from cells is required for the enhancement of therapeutic effects. In this study, we prepared nanoparticles, that arrest small-sized GSH. We modified the pores of mesoporous silica nanoparticles by the introduction of maleimide groups to react with GSH. We found that GSH was captured by the nanoparticles, while the nanoparticles did not react with the large-sized thiols such as albumin. These new nanoparticles bearing maleimide units may provide a smart molecular system with selective capturing ability of small-sized thiols under biological conditions.

INTRODUCTION

Non-protein thiols (NPSH) in tumor cells have adverse effects on cancer treatment, especially in radiation therapy.[1–4] Among several thiols in the cells, the reduced form of glutathione (GSH), typical NPSH, is known to exist in high concentration in the cells, and it plays a role in protecting intracellular molecules from damage caused by radiation.[5–8] In the light of this function, the depletion of GSH in tumor cells has been attracting attention in efforts to enhance the therapeutic effect of radiation.[9] To arrest and deactivate NPSH, several strategies have been proposed, including oxidation of thiols,[10,11] alkylation by electrophilic molecules[12–14] and prevention of NPSH synthesis.[15] However, almost all strategies influence the protein thiols nonspecifically; hence the precise arrest of small-sized NPSH remains a challenge.

These research contexts prompted us to demonstrate a selective trapping of small-sized NPSH by means of mesoporous silica nanoparticles (MSN).[16,17] Because the pores of MSN provide a limited reaction field for small molecules,[18,19] modification of the pores allows the reaction of small molecules and their capture in a selective manner. We employed maleimide groups for the arrest of NPSH, and introduced them into the pores of MSN. We prepared MSN bearing maleimide units (MSN-MI) and characterized their reaction properties.

MATERIALS AND METHODS

Fluorescence-Labeled MSN-MI (MSN-MI-F). A solution of 5-carboxyfluorescein N-succinimidyl ester (CFNSE) in mixture of DMSO (45 mL) and saturated aqueous $NaHCO_3$ (4.5 mL) was added to MSN-MI, and stirred at room temperature for 24 h. The mixture was centrifuged at 16,000 rpm for 10 min. After removing the supernatant, the mixture was washed with DMSO and water. Drying under reduced pressure afforded MSN-SMCC-F as an orange powder.

Quantification of amino and maleimide groups on MSN Surface. A solution of 5-carboxyfluorescein N-succinimidyl ester (CFNSE, 180 μM) in mixture of DMSO (45 mL) and saturated aqueous $NaHCO_3$ (4.5 mL) was added to propylamine functionalized silica nanoparticles (MSN-NH_2, 0.9 mg) or MSN-MI (0.9 mg), and the resulting mixture was stirred at room temperature for 24 h. After the reaction, the mixture was centrifuged and the supernatant was diluted 20-fold and measured by absorption spectrophotometer.

Evaluation of cellular uptake. The fluorescence labeled MSN-MI-F (0.05 mg/mL) in serum-free D-MEM was added to A549 cells, followed by incubation at 37 ˚C for 6 h. The cells was washed with PBS, and after addition of Fluoro Brite DMEM the samples were subjected to confocal microscopy.

Quantification of GSH/GSSH Ratio in Cells. Levels of GSH and GSSG were measured using a GSH/GSSG quantification kit (Dojindo, Japan). Briefly, A549 cells were pre-incubated for 24 h at 37 ˚C in 5% CO_2 and further incubated for 24 h with the medium containing MSN-MI. After washing with PBS, the cells were harvested and centrifuged for 5 min, and the supernatant was discarded. After the pellets were resuspended in 10 mM HCl (80 μL), the cell suspensions were frozen−thawed. Then, 20 μL of 5% 5- sulfosalicylic acid (SSA) was added to the suspensions and the resulting samples were centrifuged for 10 min. Then, the samples were reacted with 5, 5'-dithiobis(2-nitrobenzoic acid) (DTNB) and the absorbance at 405 nm was recorded on a microplate absorbance spectrophotometer.

Reaction of MSN-MI in lysate of A549 cells. A549 cells were pre-incubated for 48 h at 37 ˚C in 5% CO_2. After washing with PBS, the cells were harvested and centrifuged for 3 min. After the pellets were resuspended with 500 μL of H_2O, the cell suspensions were frozen−

thawed. The obtained cell lysate was incubated with MSN-MI (5.0 mg) for 30 min, and after the reaction, the samples were centrifuged at 1000 rcf. The supernatant was added to phosphate buffer (pH 8.0) and 10 mM DTNB, and the resulting mixtures were subjected a microplate absorbance spectrophotometer at 405 nm.

RESULTS AND DISCUSSION

The synthesis of MSN-MI is outlined in Figure 1. We employed commercially available MSN bearing primary amino groups (MSN-NH_2) for the preparation of MSN-MI. The size of MSN-NH_2 and their pore size were estimated to be 200 and 4 nm, respectively. Coupling of MSN-NH_2 with succinimidyl 4-(N-maleimidomethyl)cyclohexane-1-carboxylate (SMCC) gave the desired MSN-MI. Immobilization of the maleimide units on the surface of MSN was confirmed by FT-IR analysis. The strong band around 1100 cm^{-1} seems to arise from the structure of the silica nanoparticles.[20] The bands around 1680 cm^{-1} observed for MSN-MI were attributed to the C=O stretching vibration, indicating that maleimide units were immobilized on the surface of MSN. We then conducted experiments to quantify the maleimide units on the MSN. MSN-MI, or control compound MSN-NH_2, were treated with 5-carboxyfluorescein N-succinimidyl ester (CFNSE), and the resulting samples were centrifuged to yield the supernatants. The measurements of absorption spectra of supernatant revealed the amount of free CFNSE, which enabled us to estimate the amount of free amino groups on the nanoparticles. Thus, we calculated the amounts of maleimide units on MSN-MI and free amino groups on MSN-NH_2 to be 24.9 and 111.4 nmol / mg, respectively, indicating that 22% of amino groups on the surface of MSN were modified by maleimide groups. The average diameter of MSN-MI was 185.6 ± 17.5 nm as determined from TEM images (Figure 1C).

We next tracked the GSH-arrest by MSN-MI using the reaction of 5,5-dithiobis(2-nitrobenzoic acid) (DTNB). After the reaction between GSH and MSN-MI, the samples were centrifuged to obtain an unreacted GSH in supernatant, which was further reacted with DTNB. The GSH molecules in the supernatant reduced DTNB to afford 5-mercapto-2-nitrobenzoic acid (TNB), which showed typical absorption around 400-450 nm. Thus, we could monitor the reaction of MSN-MI with GSH by the measurement of absorption spectra. As shown in Figure 1D, the direct reaction of GSH with DTNB resulted in a typical strong absorption around 400-450 nm due to the formation of TNB. It is noticeable that the reaction of DTNB with a sample in which MSN-MI was mixed with GSH resulted in weak absorption. A similar reaction using the control compound N-ethyl maleimide (NEM), which is a trapping reagent of GSH, also showed weak absorption, indicating that MSN-MI arrested GSH in a similar efficiency of

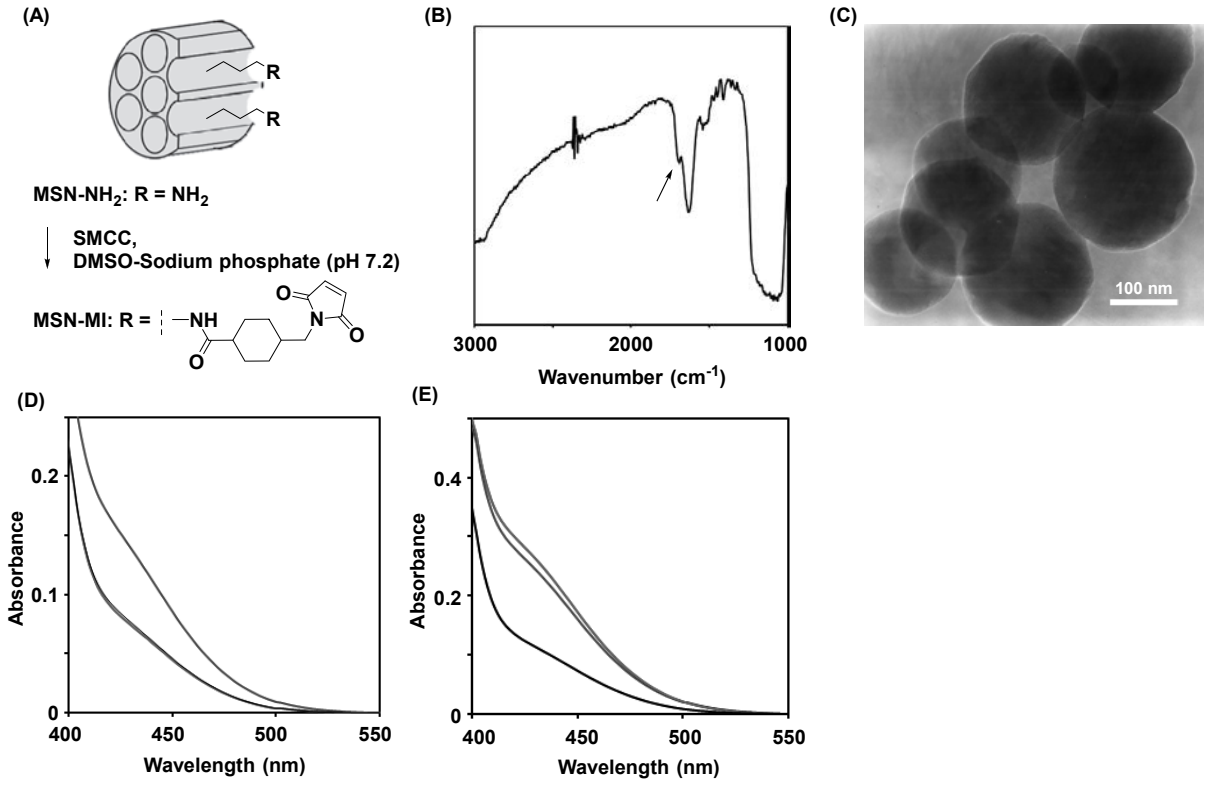

Figure 1. (A) Synthesis of MSN-MI using succinimidyl 4-(N-maleimidomethyl)cyclohexane-1-carboxylate (SMCC). (B) FT-IR spectra of MSN-MI. Arrow indicates C=O vibration. (C) TEM images of MSN-MI (Avg. 185.6 nm, S.D. 17.5 nm). (D, E) Absorption spectra of DTNB after the reaction of thiols (D: GSH, E: BSA). After the reaction of GSH (100 μM) or BSA (100 μM) with MSN-MI (1 mg, red) or NEM (25 nmol, black), the samples were centrifuged to obtain an unreacted thiols in supernatant, which was further reacted with DTNB. Absorption spectra of control samples (direct treatment of thiols with DTNB) were depicted in blue line.

NEM. In separate experiments, we monitored the reaction of bovine serum albumin (BSA), which consists of 853 amino acids with one free cysteine.[21–22] The Stokes radius of the BSA molecule is estimated to be 3.55 nm;[23] hence, BSA could not enter the pores of MSN-MI to react with the maleimide units. We observed that the reaction of DTNB with the sample obtained from the reaction of MSN-MI and BSA showed strong absorption, similar to that of the sample obtained from the reaction of DTNB and BSA itself (Figure 1E). Given that BSA reacted with NEM to show weak absorption, it is reasonable to conclude that MSN-MI arrested small GSH in a selective manner due to the size effect of the pores.

For a better understanding of the function of MSN-MI in living cells, we next assessed the cellular uptake of MSN-MI using a human cell line of lung carcinoma A549 cells. Fluorescein-labeled MSN-MI (MSN-MI-F) was prepared to track their cellular dynamics and was administered to A549 cells. As shown in Figure 2A, we observed bright emission of fluorescein on MSN-MI from the cells. We confirmed that MSN-MI-F was accumulated in cytosol in the cells by co-stained experiments. We examined the merged images of fluorescence of MSN-MI-F and organelle-specific fluorescent molecules, which targeted nucleus, lysosome and cell membrane. We did not observe a merged color of MSN-MI-F and other fluorescent agents, indicating that MSN-MI-F had access to the cytosol but not to the lysosome. We next evaluated the GSH arrest by MSN-MI in A549 cells. After incubation of the cells for 24 h in the presence of MSN-MI, the ratio of GSH and GSSG (GSH / GSSG) in the cells was quantified. Although a decrease of the amount of GSH was expected because of the function of MSN-MI, we observed no effect on the GSH / GSSG ratio (Figure 2B). To confirm whether the GSH arrest can occur within cells, we further studied the reaction of MSN-MI upon treatment with cell lysate. After a solution of MSN-MI was incubated with the lysate of A549 cells, the amount of thiols in the cell

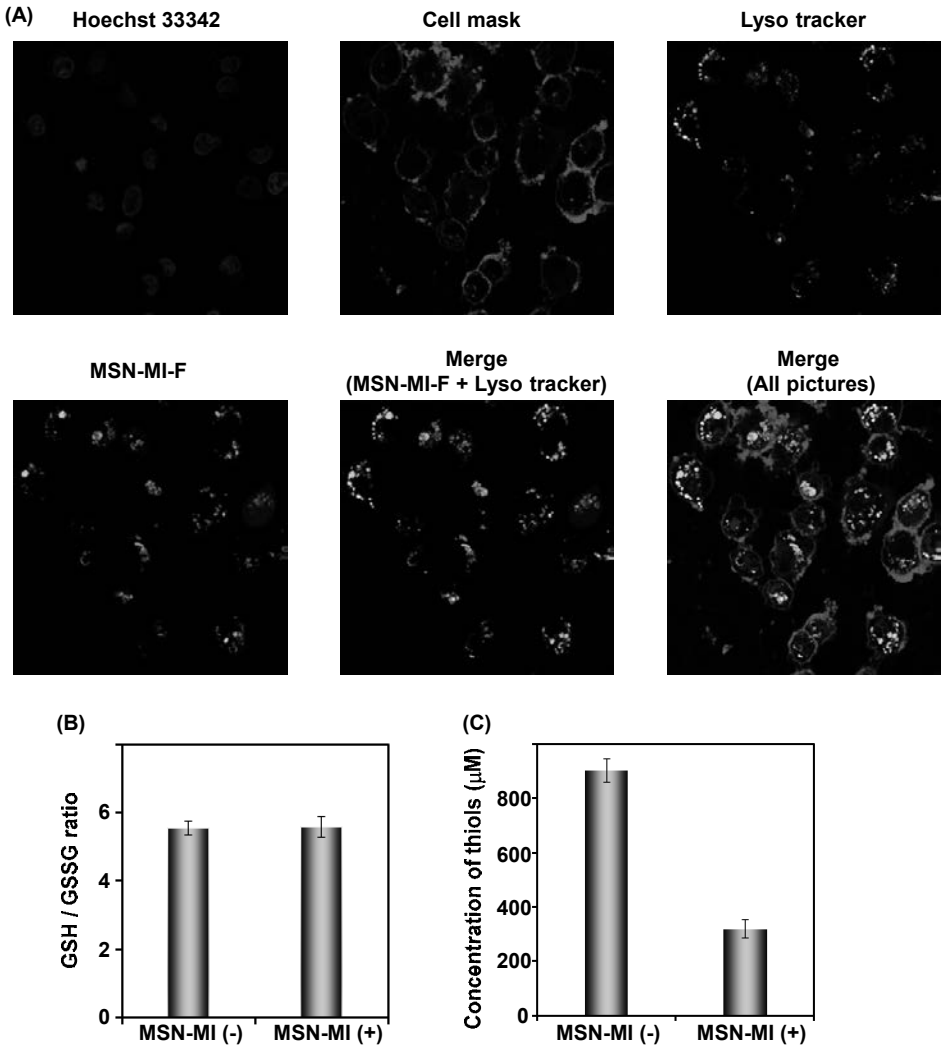

Figure 2. (A) Localization of MSN-MI-F in A549 cells. The cells were incubated with MSN-MI-F (green) and then nucleus (blue), cell membrane (red) and lysosome (light blue) were stained by organelle markers, Hoechst 33342, Cell mask and Lyso tracker, respectively. (B) GSH/GSSG ratio in A549 cells before or after treatment with MSN-MI (0.2 mg / mL) for 24 h at 37 ℃. (C) Concentration of thiols in the lysate of A549 cells before or after treatment MSNMI (5 mg) for 30 min at 37 ℃.

lysate was determined. As shown in Figure 2C, an evident decrease of thiols was observed in the sample treated with MSN-MI, indicating that MSN-MI maintained the GSH arresting function even in the cells. At present, the reason for the ineffectiveness of MSN-MI in living cells is unclear, however, the one acceptable explanation is that the cellular uptake of MSN-MI was not sufficient to express their original capturing ability for GSH.

CONCLUSION

In summary, in an effort to improve the radiosensitivity of tumor cells, we attempted to design a molecular system for capturing intracellular non-protein thiols such as GSH. We synthesized mesoporous silica nanoparticles, that had their pores modified by maleimide units (MSN-MI) and characterized their reactivity toward GSH. MSN-MI captured small GSH in the pores, while the large-sized thiols did not react with MSN-MI because they could not enter the pores. Although MSN-MI appeared to be promising as an agent to trap GSH, results of cellular experiments revealed that MSN-MI did not function in living cells, probably due to the low cellular uptake. Improvements to enhance the uptake and attainment of efficient accumulation of MSN-MI in the cells by the surface modification of nanoparticles are currently underway.

REFERENCES

1. Balendiran G. K., Dabur R., Fraser D. The role of glutathione in cancer. *Cell Biochem. Fucnt.* 2004; 22: 343.
2. Estrela J. M., Ortega A., Obrador E. Glutathione in cancer biology and therapy. *Crit. Rev. Clin. Lab. Sci.* 2006; 43: 143.
3. Ishimoto T., Nagano O., Yae T., Tamada M., Motohara T., Oshima H., Oshima M., Ikeda T., Asaba R., Yagi H., Masuko T., Shimizu T., Ishikawa T., Kai K., Takahashi E., Imamura Y., Baba Y., Ohmura M., Suematsu M., Baba H., Saya H. CD44 variant regulates redox status in cancer cells by stabilizing the xCT subunit of system xc(-) and thereby promotes tumor growth. *Cancer Cell* 2011; 19: 387.
4. Lipard M., Bothe E., Schulte-frohlinde D. Determination of the Constants of the Alper Formula for Single-strand Breaks from Kinetic Measurements on DNA in Aqueous Solution and Comparison with Data from Cells. *Int. J. Radiat. Biol.* 1990; 58: 603.
5. Alper T.; *Cellular Radiobiology.* Cambridge University Press: Cambridge, 1979.
6. Astor M. B.; Anderson V.; Mester A. Relationship between intracellular GSH levels and hypoxic cell radiosensitivity. *Pharmaco. Ther.* 1988; 39: 115.
7. Held K. D. Models for thiol protection of DNA in cells. *Pharmaco. Ther.* 1988; 39: 123.
8. Chapman J. D., Greenstock C. L., Reuvers A. P., Dugle D. L. The Inactivation of Chinese Hamster Cells by X Rays: The Effects of Chemical Modifiers on Single- and Double-Events. *Radiat. Res.* 1975; 64: 365.
9. Zhang X., Chen X., Jiang Y. –W., Ma N., Xia L. –Y., Cheng X., Jia H. –R., Liu P., Gu, N., Chen Z., We F. –G. Glutathione-Depleting Gold Nanoclusters for Enhanced Cancer Radiotherapy through Synergistic External and Internal Regulations. *ACS Appl. Mater. Interfaces* 2018; 10: 10601.
10. Lin L. –S., Song J., Song, L., Ke K., Liu Y., Zhou Z., Shen Z., Shen Z., Li J., Yang Z., Tang W., Niu G., Yang H. –H., Chen X. Simultaneous Fenton-like Ion Delivery and Glutathione Depletion by MnO_2-Based Nanoagent to Enhance Chemodynamic Therapy. *Angew. Chem. Int. Ed.* 2018; *57*: 4902.
11. Harris J. W., Power J. A. Diamide: A New Radiosensitizer for Anoxic Cells. *Radiat. Res.* 1973; 56: 97.
12. Han A., Sinclair W. K., Kimler B. F. The Effect of N-Ethylmaleimide on the Response to X Rays of Synchronized HeLa Cells. *Radiat. Res.* 1976; 65: 337.
13. Nishimoto S., Zhou L. Cellular non-protein thiol depletion and radiosensitization of hypoxic cells by a novel 2-nitroimidazole derivative possessing an NPSH-reactive side chain. *Bioorg. Med. Chem. Lett.* 1994; 4: 439.
14. Tanabe K., Kojima R., Hatta H., Nishimoto S. Propargylic sulfones possessing a 2-nitroimidazole function: novel hypoxic-cell radiosensitizers with intracellular non-protein thiol depletion ability. *Bioorg. Med. Chem. Lett.* 2004; 14: 2633.
15. Biaglow J. E., Varnes M. E., Clark E. P., Epp E. R. The Role of Thiols in Cellular Response to Radiation and Drugs. *Radiat. Res.* 1983; 95: 437.
16. Li Z., Barnes J. C., Bosoy A., Stoddart J. F., Zink J. I. Mesoporous silica nanoparticles in biomedical applications. *Chem. Soc. Rev.* 2012; 41: 2590.
17. Wu S. –H., Hung Y., Mou C. –Y. Mesoporous silica nanoparticles as nanocarriers. *Chem. Commun*. 2011; 47: 9972.
18. Nakamura T., Son A., Umehara Y., Ito T., Kurihara R., Ikemura Y., Tanabe K. Confined Singlet Oxygen in Mesoporous Silica Nanoparticles: Selective Photochemical Oxidation of Small Molecules in Living Cells. *Bioconjugate Chem.* 2016; 27: 1058.
19. Umehara Y., Son A., Kondo T., Tanabe K. Dioxetane formation and chemiluminescent emission upon the combination of a vinylphenol derivative with naphthalene endoperoxide. *RSC advances* 2017; 7: 9472.
20. Shawky S. M., Abo-AlHassan A. A., Lill H., Bald D., EL-Khamisy S. F., Ebeid E. –Z. M. Efficient Loading and Encapsulation of Anti-Tuberculosis Drugs using Multifunctional Mesoporous Silicate Nanoparticles. *J. Nanosci. Curr. Res.* 2016; 1: 1000103.
21. Rombouts I., Lagrain B., Scherf K. A., Lambrecht M. A., Koehler P., Delcour J. A. Formation and reshuffling of disulfide bonds in bovine serum albumin

demonstrated using tandem mass spectrometry with collision-induced and electron-transfer dissociation. *Sci. Rep.* 2015; 5: 12210.
22. Paris G., Kraszewski S., Ramseyer C., Enescu M. About the structural role of disulfide bridges in serum albumins: Evidence from protein simulated unfolding. *Biopolymers* 2012; 97: 889.
23. Erickson H. P. Size and Shape of Protein Molecules at the Nanometer Level Determined by Sedimentation, Gel Filtration, and Electron Microscopy. *Biol. Proced Online*, 2009; 11: 32.

Possible beneficial effects of narrow-band UVB therapy on hypertension and vitamin D levels in patients with cutaneous disease

Takuo Emoto[1], Naoto Sasaki[1,2], Tomoya Yamashita[1], Atsushi Fukunaga[3], Taro Masaki[3], Chikako Nishigori[3], Ken-ichi Hirata[1]

[1]Division of Cardiovascular Medicine, Department of Internal Medicine, Kobe University Graduate School of Medicine, Kobe, Japan
[2]Laboratory of Medical Pharmaceutics, Kobe Pharmaceutical University, Kobe, Japan
[3]Division of Dermatology, Department of Internal Related, Kobe University Graduate School of Medicine, Kobe, Japan

Address correspondence to:

Naoto Sasaki, MD, PhD. E-mail: n-sasaki@kobepharma-u.ac.jp
Laboratory of Medical Pharmaceutics, Kobe Pharmaceutical University, 4-19-1, Motoyamakita-machi, Higashinada-ku, Kobe, 658-8558, Japan.
Telephone number; +81-78-441-7579, FAX number; +81-78-441-7579

Abstract

Epidemiological studies show a possible link between cardiovascular disease, hypertension, and low vitamin D levels partly due to limited sunlight exposure. We previously demonstrated that UVB exposure prevents atherosclerosis in mice by suppressing T-cell-mediated immunoinflammatory responses. Phototherapy using UVB radiation is an established treatment for immunoinflammatory cutaneous disorders. However, it remains unknown whether UVB irradiation prevents atherosclerotic cardiovascular disease and hypertension in humans. We investigated the effect of narrow-band (NB)-UVB irradiation on vascular function, blood pressure, T-cell immune responses, and vitamin D levels in patients with cutaneous diseases. Although NB-UVB did not affect vascular function in the brachial artery, it tended to decrease systolic blood pressure in three hypertensive patients. Peripheral regulatory and effector T cells were not significantly affected by NB-UVB therapy. NB-UVB significantly increased serum 1,25-dihydroxyvitamin D levels and tended to increase serum 25-hydroxyvitamin D levels. Although the sample size is small, our data suggest that NB-UVB therapy may have beneficial effects on hypertension and anti-inflammatory vitamin D levels.

Key words: narrow band UVB, cardiovascular disease, hypertension, T cells, vitamin D

Introduction

Despite advances in pharmaceutical treatment for lifestyle-associated risk factors such as hyperlipidemia, diabetes, and hypertension, atherosclerotic cardiovascular disease is a major cause of mortality in developed countries. Importantly, a large number of patients suffer from uncontrollable hypertension. Therefore, it is important to develop novel therapeutic approaches for preventing these diseases.

Recent experimental and clinical evidence suggests that innate and adaptive immune responses contribute to vascular wall inflammation and play important roles in the development and progression of atherosclerotic cardiovascular disease[1] and hypertension.[2] We and others have shown the involvement of the imbalance between proatherogenic effector T cells (Teffs) and atheroprotective regulatory T cells (Tregs), which are known to regulate excessive immune responses,[3] in the pathogenesis of atherosclerotic disease[4, 5] and hypertension.[2] Numerous animal studies have demonstrated that modulation of the Treg/Teff balance, by suppressing Teff responses and promoting Treg responses, can prevent atherosclerotic disease[6-8] and hypertension.[9, 10]

Recent experimental and epidemiological studies have suggested a possible role of vitamin D in prevention of atherosclerotic cardiovascular disease and hypertension.[11-14] Epidemiological studies show a possible link between cardiovascular disease, hypertension, and sunlight exposure.[15-17] This phenomenon may be attributable to low levels of anti-inflammatory vitamin D, because UVB exposure to the skin plays a critical role in the synthesis of vitamin D. We recently demonstrated that in addition to its possible protective role against atherosclerosis and hypertension by promoting vitamin D production, broad-band (BB)-UVB irradiation prevents experimental atherosclerosis and abdominal aortic aneurysm by expanding atheroprotective Tregs, suggesting a novel immunomodulatory strategy to prevent atherosclerotic cardiovascular disease.[18-20] UVB irradiation is reported to critically regulate the immune system[21] and is clinically used for the treatment of cutaneous diseases such as psoriasis and atopic dermatitis. However, it remains unknown whether UVB irradiation prevents

atherosclerotic cardiovascular disease and hypertension in humans.

In the present study, we investigated the effect of narrow-band (NB)-UVB irradiation, the most frequently used UVB wavelength for treatment of cutaneous disease, on vascular function, blood pressure, T-cell immune responses, and vitamin D levels in patients with cutaneous disease.

Methods

Recruitment of Patients

Patients with psoriasis, atopic dermatitis, and other cutaneous diseases, who underwent NB-UVB therapy for the first time or after at least six months interval, were recruited from Kobe University Hospital. Patients with systemic diseases including hepatic disease, renal disease (serum creatinine levels > 2.0 mg/dL), and malignancy were excluded. This study was performed in compliance with the Declaration of Helsinki and was approved by the Ethics Committee of Kobe University (No.1530). All subjects provided oral and written informed consent to participate in this study. We determined the patient's minimal erythema dose (MED) to establish the optimal dosage schedule prior to phototherapy (330-480mJ/cm^2/once). Patients were treated once to three times per week, depending on the severity of cutaneous diseases and their life style.

Flow-mediated Dilatation (FMD) and Blood Pressure

The %FMD change in the brachial artery diameter was computed from initial and maximum diameters after the cuff occlusion as described previously.[22] Systolic and diastolic blood pressure was measured on three consecutive days in the morning before breakfast at home and was compared between baseline and three months after UVB therapy.

Flow Cytometric Analysis

Peripheral blood samples of patients were obtained in EDTA-coated tubes. Peripheral blood mononuclear cells were prepared by Ficoll gradient centrifugation and incubated in phosphate-buffered saline containing 2% fetal calf serum. Fluorescent-activated cell sorter analysis was performed by Attune Acoustic Focusing Cytometer (Life Technologies, Carlsbad, CA) using FlowJo10.0.6 software (Tree Star). The antibodies used were as follows; PerCPCy5.5-anti-CD3 (clone SK7; BD Biosciences), APCCy7-anti-CD4 (clone RPA-T4; BD Biosciences), APC-anti-FoxP3 (clone 236A/E7; Biosciences), PECy7-anti-CD45RA (clone L48; BD Biosciences) and isotype-matched control antibodies.

Measurement of Serum Vitamin D

Serum 1,25-dihydroxyvitamin D and 25-hydroxyvitamin D were analyzed by radioimmunoassay as described previously (SRL, Tokyo, Japan).[11]

Statistical Analysis

Data represent the mean ± S.D. Paired *t* test was used for statistical correlation between pre and post NB-UVB therapy. All statistical analyses were two sided; $P < 0.05$ was considered statistically significant. For statistical analysis, GraphPad Prism version 7.0 (GraphPad Software, San Diego, CA, USA) was used.

Results and Discussion

The baseline characteristics were presented in Table. Three patients with hypertension were included in this study. The dose and frequency of NB-UVB therapy were determined depending on minimal erythema dose and severity of the disease. We examined the effect of NB-UVB therapy on vascular function and blood pressure. FMD, which is considered to be one of the most reliable non-invasive methods for detecting early stages of atherosclerosis, was not affected by NB-UVB therapy (Figure 1A). Interestingly, systolic blood pressure tended

Table. Baseline characteristics

Patients	Age	Sex	Disease	Dose of NB-UVB (mJ/cm^2/once)	Frequency (per week)	Hypertension
No.1	87	Male	Psoriasis	330	2	−
No.2	30	Male	Atopic dermatitis	400	1	−
No.3	43	Male	Atopic dermatitis	400	3 (8weeks), 1 (4weeks)	−
No.4	30	Male	Atopic dermatitis	400	3 (8weeks), 1 (4weeks)	−
No.5	70	Male	Psoriasis	350	3	+
No.6	59	Female	Another disease	400	1 or 2	+
No.7	72	Male	Psoriasis	480	1	+
No.8	82	Male	Psoriasis	300	1	−

Hypertension was defined as blood pressure > 140/90 mmHg.

to be decreased in three hypertensive patients following NB-UVB therapy (163 ± 3 mmHg to 149 ± 6mmHg, P = 0.06) (Figure 1B).

Epidemiological studies suggest a possible association between cardiovascular disease, hypertension, and sunlight exposure,[15-17] which may be partly explained by limited UVB exposure. However, there is no report providing direct evidence that UVB prevents these diseases. Interestingly, in this study, we showed the possibility that NB-UVB therapy may contribute to the improvement of hypertension in patients with cutaneous disease, although it did not affect FMD in the brachial artery, an indicator for early stages of atherosclerosis.

Recent experimental and clinical evidence shows an imbalance between proatherogenic Teffs and atheroprotective Tregs in atherosclerotic cardiovascular disease and hypertension.[2, 5] Earlier clinical studies showed that bath-psoralen UVA or NB-UVB therapy expanded $CD4^+CD25^+Foxp3^+$ Tregs in the peripheral blood of patients with skin autoimmune disease.[23, 24] Our recent experimental study demonstrated that BB-UVB irradiation to the murine skin prevented the development of atherosclerosis and abdominal aortic aneurysm by favorably modulating the balance between Teffs and Tregs.[18, 19] Therefore, we next investigated the effect of NB-UVB on these T-cell immune responses by flow cytometry, and found that the proportions of resting Tregs (Fr1), activated Tregs (Fr2), and Treg/Teff ratio (Fr1+2 / Fr3+4+5) were not affected by NB-UVB therapy (Figure 2A and 2B). Importantly, BB-UVB (a continuous spectrum from 280 to 320 nm with a peak around 313 nm) was used in our animal studies, whereas in this clinical study we used NB-UVB (a narrow peak around 311 nm). We speculate that there might be some differences in the beneficial effects of UVB on Treg immune responses depending on its wavelength, although differences in the immunological anti-inflammatory actions between BB-UVB and NB-UVB have not been clarified. Moreover, because as shown in Table, the dosage and frequency of NB-UVB therapy differed considerably among patients in this study, we could not discuss the dose-dependent effect of NB-UVB therapy. Collectively, the discrepancy between our data and the previous reports may potentially be due to very small number of patients, or the differences in UVB dose, wavelength, or protocol and patient characteristics, and further studies will be required.

Accumulating clinical evidence highlights the vitamin D deficiency and a predisposition to cardiovascular events and hypertension.[12, 14] In addition, our previous study using atherosclerotic mice showed anti-atherogenic properties of biologically active 1,25-dihydroxyvitamin D.[11] In addition to its dietary intake, the synthesis of vitamin D in the UVB-exposed skin are known to play a major role in the maintenance of its systemic levels. In consideration of these backgrounds, it is likely that possible protective roles of UVB in cardiovascular disease and hypertension may be partly due to increased vitamin D production. We examined the effect of NB-UVB on serum vitamin D levels. Serum levels of biologically active 1,25-dihydroxyvitamin D were significantly increased (53.2 ± 16.2 ng/ml to 67.1 ± 14.3 ng/ml, P = 0.03), and those of storage form 25-hydroxy vitamin D were tended to be increased following NB-UVB therapy (18.3 ± 12.7 pg/ml to 36.3 ± 17.8 pg/ml, p = 0.05) (Figure 3). These data are consistent with a previous report evaluating the influence of NB-UVB therapy on serum 25-hydroxy vitamin D levels in patients with skin diseases.[25] Although no prior work has examined serum 1,25-dihydroxyvitamin D levels in patients with skin diseases, a recent study showed that NB-UVB exposure significantly increased serum 1,25-dihydroxyvitamin D levels as well as 25-hydroxy vitamin D levels in chronic kidney disease

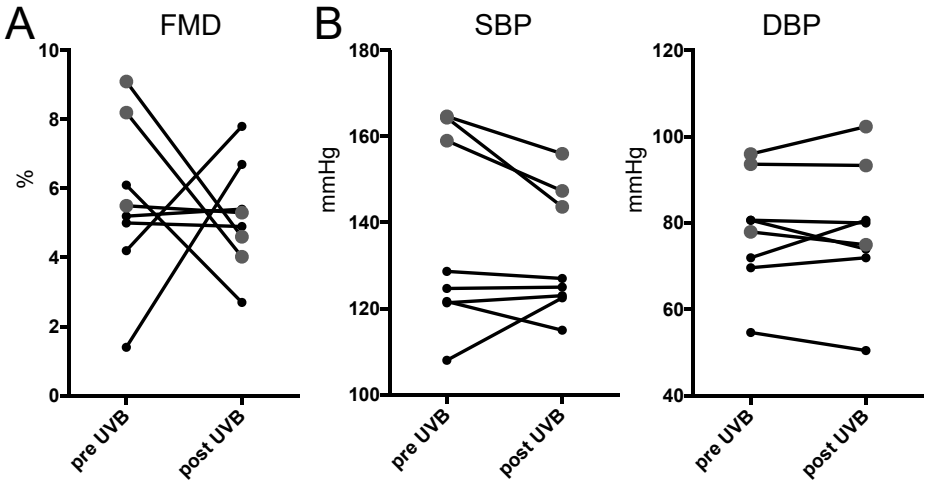

Figure 1. Flow-mediated dilatation (FMD) and Blood pressure.
(A) FMD was not affected by NB-UVB therapy. (B) Narrow-band (NV) UVB therapy tended to lower systolic blood pressure (SBP) (from 163 ± 3 mmHg to 149 ± 6 mmHg, P = 0.06) in three hypertensive patients, but not in normotensive patients. Blood pressure was measured on 3 consecutive days in the morning before breakfast at home and averaged. DBP, diastolic blood pressure. The data in hypertensive patients are shown in red.

patients on dialysis.[26] To our knowledge, this is the first report demonstrating increased production of biologically active 1,25-dihydroxyvitamin D following NB-UVB therapy in patients with skin diseases. Our data indicate the possible involvement of promoted vitamin D production in NB-UVB-dependent protection against hypertension in patients with cutaneous diseases. However, protective roles of vitamin D against hypertension remains to be determined, because a recent prospective, randomized trial failed to show beneficial effects of oral vitamin D supplementation on blood pressure in individuals who have low serum concentrations of 25-hydroxyvitamin D and elevated blood pressure.[27] Future clinical studies should provide direct evidence for anti-hypertensive effects of vitamin D.

This study included some limitations. First, the number of patients was too small to draw conclusions about the beneficial effects of NB-UVB therapy on hypertension. Second, some patients had normal blood pressure and vascular function. Third, there were differences in NB-UVB irradiation dose or frequency among patients. Based on our findings, additional larger trials including patients

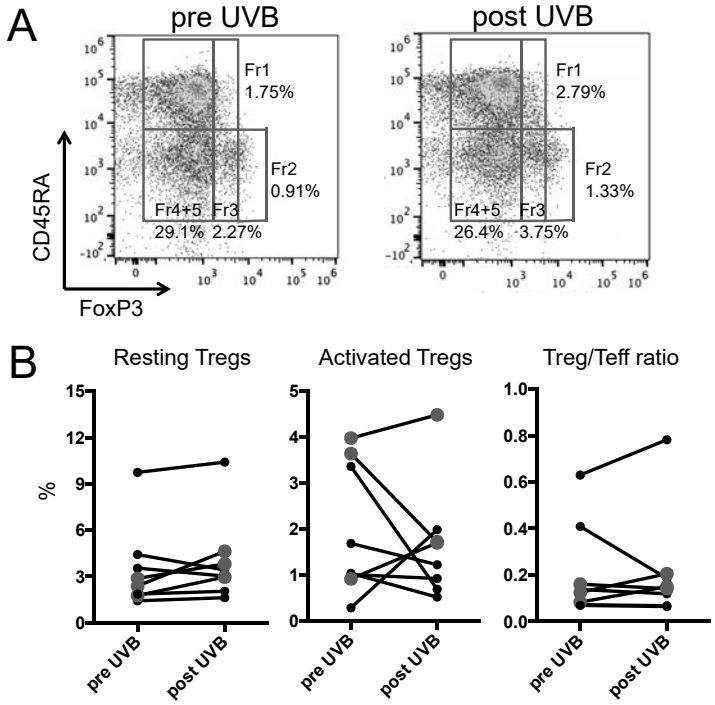

Figure 2. Regulatory T cells (Tregs) and effector T cells (Teffs).
(A) Representative flow cytometric analysis of Tregs and Teffs. (B) Resting Tregs, activated Tregs, and Treg/Teff ratio were not changed after NB-UVB therapy. Treg/Teff ratio was calculated by Fr1+2 / Fr3+4+5. Fr1, resting Tregs; Fr2, activated Tregs; Fr3, Teffs; and Fr4+5, Teffs. The data in hypertensive patients are shown in red.

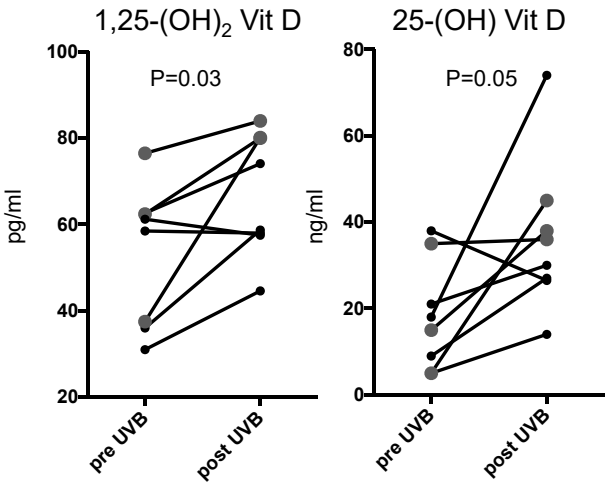

Figure 3. Serum vitamin D levels.
Serum levels of biologically active 1,25-dihydroxyvitamin D (1,25-$(OH)_2$ Vit D) were significantly increased, and those of storage form 25-hydroxyvitamin D (25-(OH) Vit D) tended to be increased following NB-UVB therapy. The data in hypertensive patients are shown in red.

with hypertension or atherosclerotic cardiovascular disease are needed to validate our observations.

Although larger clinical trials should be conducted, our data suggest that NB-UVB therapy can systemically increase vitamin D and may have beneficial effects on hypertension.

Sources of Funding

This work was supported by JSPS KAKENHI Grant Numbers 25860601 (N. Sasaki) and 15K09156 (N. Sasaki).

Clinical Trial Registration Information:

URL: http://www.umin.ac.jp/ctr/. Unique identifier: UMIN000015422.

Disclosures

None.

References

1. Hansson GK, Hermansson A. The immune system in atherosclerosis. Nat Immunol. 2011;12:204-212.
2. McMaster WG, Kirabo A, Madhur MS, Harrison DG. Inflammation, immunity, and hypertensive end-organ damage. Circ Res. 2015;116:1022-1033.
3. Sakaguchi S, Yamaguchi T, Nomura T, Ono M. Regulatory T cells and immune tolerance. Cell. 2008;133:775-787.
4. Emoto T, Sasaki N, Yamashita T, et al. Regulatory/effector T-cell ratio is reduced in coronary artery disease. Circ J. 2014;78:2935-2941.
5. Sasaki N, Yamashita T, Kasahara K, Takeda M, Hirata K. Regulatory T cells and tolerogenic dendritic cells as critical immune modulators in atherogenesis. Curr Pharm Des. 2015;21:1107-1117.
6. Sasaki N, Yamashita T, Takeda M, et al. Oral anti-CD3 antibody treatment induces regulatory T cells and inhibits the development of atherosclerosis in mice. Circulation. 2009;120:1996-2005.
7. Kasahara K, Sasaki N, Yamashita T, et al. CD3 antibody and IL-2 complex combination therapy inhibits atherosclerosis by augmenting a regulatory immune response. J Am Heart Assoc. 2014;3:e000719.
8. Matsumoto T, Sasaki N, Yamashita T, et al. Overexpression of cytotoxic T-lymphocyte-associated antigen-4 prevents atherosclerosis in mice. Arterioscler Thromb Vasc Biol. 2016;36:1141-1151.
9. Vinh A, Chen W, Blinder Y, et al. Inhibition and genetic ablation of the B7/CD28 T-cell costimulation axis prevents experimental hypertension. Circulation. 2010;122:2529-2537.
10. Barhoumi T, Kasal DA, Li MW, et al. T regulatory lymphocytes prevent angiotensin II-induced hypertension and vascular injury. Hypertension. 2011;57:469-476.
11. Takeda M, Yamashita T, Sasaki N, et al. Oral administration of an active form of vitamin D3 (calcitriol) decreases atherosclerosis in mice by inducing regulatory T cells and immature dendritic cells with tolerogenic functions. Arterioscler Thromb Vasc Biol. 2010;30:2495-2503.
12. Wang TJ, Pencina MJ, Booth SL, et al. Vitamin D deficiency and risk of cardiovascular disease. Circulation. 2008;117:503-511.
13. Weng S, Sprague JE, Oh J, et al. Vitamin D deficiency induces high blood pressure and accelerates atherosclerosis in mice. PloS one. 2013;8:e54625.
14. Forman JP, Giovannucci E, Holmes MD, et al. Plasma 25-hydroxyvitamin D levels and risk of incident hypertension. Hypertension. 2007;49:1063-1069.
15. Voors AW, Johnson WD. Altitude and arteriosclerotic heart disease mortality in white residents of 99 of the 100 largest cities in the United States. J Chronic Dis. 1979;32:157-162.
16. Scragg R. Seasonality of cardiovascular disease mortality and the possible protective effect of ultraviolet radiation. Int J Epidemiol. 1981;10:337-341.
17. Rostand SG. Ultraviolet light may contribute to geographic and racial blood pressure differences. Hypertension. 1997;30:150-156.
18. Sasaki N, Yamashita T, Kasahara K, et al. UVB exposure prevents atherosclerosis by regulating immunoinflammatory responses. Arterioscler Thromb Vasc Biol. 2017;37:66-74.
19. Hayashi T, Sasaki N, Yamashita T, et al. Ultraviolet B exposure inhibits angiotensin II-induced abdominal aortic aneurysm formation in mice by expanding $CD4^{+}Foxp3^{+}$ regulatory T cells. J Am Heart Assoc. 2017;6.
20. Sasaki N, Yamashita T, Takeda M, Hirata K. Regulatory T cells in atherogenesis. J Atheroscler Thromb. 2012;19:503-515.
21. Schwarz T. Mechanisms of UV-induced immunosuppression. Keio J Med. 2005;54:165-171.
22. Emoto T, Sawada T, Hashimoto M, et al. Effect of 3-month repeated administration of miglitol on vascular endothelial function in patients with diabetes mellitus and coronary artery disease. Am J Cardiol. 2012;109:42-46.
23. Furuhashi T, Saito C, Torii K, Nishida E, Yamazaki S, Morita A. Photo(chemo)therapy reduces circulating Th17 cells and restores circulating regulatory T cells in psoriasis. PloS one. 2013;8:e54895.
24. Iyama S, Murase K, Sato T, et al. Narrowband ultraviolet B phototherapy ameliorates acute graft-versus-host disease by a mechanism involving in vivo expansion of CD4+CD25+Foxp3+ regulatory T cells. Int J Hematol. 2014;99:471-476.
25. Cicarma E, Mork C, Porojnicu AC, et al. Influence of narrowband UVB phototherapy on vitamin D and folate status. Exp Dermatol. 2010;19:e67-72.
26. Ala-Houhala MJ, Vahavihu K, Hasan T, et al. Narrow-band ultraviolet B exposure increases serum vitamin

D levels in haemodialysis patients. Nephrol Dial Transplant. 2012;27:2435-2440.
27. Arora P, Song Y, Dusek J, et al. Vitamin D therapy in individuals with prehypertension or hypertension: The daylight trial. Circulation. 2015;131:254-262.

光老化は毎日のUVケアで防ぐことができます。

患者様に必要なのは、肌にやさしく、紫外線を確実に防ぐことです。

顔もからだも、毎日頼れるSPF50+

汗・水に強く、美しい仕上がりが一日続く日やけ止め。

アクセーヌ スーパーサンシールド ブライトフィット
(日やけ止め乳液)顔・からだ用

SPF50+ PA++++ 40g 3,000円(税抜)

紫外線吸収剤フリー・低刺激性・無香料・アルコール(エタノール)フリー・
パラベンフリー・ノンコメドジェニックテスト済* ・ウォータープルーフタイプ
色素を薄膜シリカでコーティングする技術<パーフェクトヴェール>採用
石けんなどの洗浄剤で落とせます。
*すべての方に、肌トラブルが起こらない、ニキビのもと(コメド)ができないというわけではありません。

アクセーヌ スーパーサンシールド ブライトフィット 特長

汗・水に強く、紫外線遮蔽効果を持続しながらみずみずしく潤う。独自技術<MCキトサンヴェール>採用。
エモリエント成分でコーティングした紫外線散乱剤が肌に負担なくなめらかにのび、均一に密着。
べたつかない心地よい使用感を実現したウォーターベース処方。

約9割が「のびがよい」「肌に負担がかからない」と回答。

皮膚科通院歴のある方への使用評価(アクセーヌ調べ・27名)

のびがよい	肌に負担がかからない	しっとりとした使い心地
90%	87%	85%

ACS アクセーヌ製品は皮膚科医と共同で研究に取り組んだACSの考え方に基づいて開発されています。
ACSとは化粧品や日常の生活品の中から、できるだけ刺激物質を取り除き、肌の健康を保つシステムのことです。

光老化
ひかりろうか
アクセーヌ株式会社は「光老化啓発プロジェクト」に協賛しています。

■ 製品資料・サンプルのご送付や院内でのご販売について等のお問い合わせ
アクセーヌ株式会社　学術グループ　531-0072　大阪市北区豊崎3-19-3
TEL:0120-823341　FAX:0120-555949　アクセーヌ カスタマーセンターのオペレーターがご依頼を承ります。

■ 医療関係者様向け情報　アクセーヌ 医療関係　検索

ACSEINE

ヒト化抗ヒト IL-17Aモノクローナル抗体製剤

生物由来製品・劇薬・処方箋医薬品*

トルツ® 皮下注 80mg オートインジェクター
皮下注 80mg シリンジ

taltz® (ixekizumab) injection

イキセキズマブ（遺伝子組換え）注射液

薬価基準収載

＊注意－医師等の処方箋により使用すること

効能・効果、用法・用量、警告・禁忌を含む使用上の注意等については、製品添付文書をご参照ください。

●トルツ®の情報はインターネットでご覧になれます。

医療従事者向け https://taltz-doctor.jp

患者さん向け https://taltz-patient.jp

製造販売元（資料請求先）
日本イーライリリー株式会社
〒651-0086 神戸市中央区磯上通5丁目1番28号

販売提携（資料請求先）
鳥居薬品株式会社
東京都中央区日本橋本町３-４-１

TAL-A031（R2）
2018年8月作成

協和発酵キリン株式会社
http://www.kyowa-kirin.co.jp

たった一度のいのちと歩く。

KYOWA KIRIN

私たちの志　検索

2015年12月作成

【禁忌(次の患者には投与しないこと)】
1.本剤の成分に対し過敏症の既往歴のある患者
2.妊婦又は妊娠している可能性のある女性[(「妊婦、産婦、授乳婦等への投与」の項参照)]

【効能・効果】
局所療法で効果不十分な尋常性乾癬
関節症性乾癬

《効能・効果に関連する使用上の注意》
以下のいずれかを満たす尋常性乾癬又は関節症性乾癬患者に投与すること。
(1)ステロイド外用剤等で十分な効果が得られず、皮疹が体表面積の10%以上に及ぶ患者
(2)難治性の皮疹又は関節症状を有する患者

【用法・用量】
通常、成人にはアプレミラストとして以下のとおり経口投与し、6日目以降はアプレミラストとして1回30mgを1日2回、朝夕に経口投与する。

1日目	2日目		3日目		4日目		5日目		6日目以降	
朝	朝	夕	朝	夕	朝	夕	朝	夕	朝	夕
10mg	10mg	10mg	10mg	20mg	20mg	20mg	20mg	30mg	30mg	30mg

《用法・用量に関連する使用上の注意》
(1)投与開始時に漸増投与を行わなかった場合、悪心、下痢、嘔吐等の発現率が高いことが示されているため、「用法・用量」を遵守すること。
(2)重度の腎機能障害患者(Cockcroft-Gault式によるクレアチニンクリアランス値が30mL/min未満)では、本剤の血中濃度が上昇する可能性があることから、本剤を30mg1日1回投与する等、減量も考慮し、慎重に投与すること。なお、本剤30mg1日1回投与とする場合、投与開始時は朝の用量のみ投与すること。[「慎重投与」「薬物動態」の項参照]
(3)本剤による治療反応は、通常投与開始から24週以内に得られる。24週以内に治療反応が得られない場合は、本剤の治療計画の継続を慎重に再考すること。

【使用上の注意】
1. 慎重投与(次の患者には慎重に投与すること)
1)重度の腎機能障害(Cockcroft-Gault式によるクレアチニンクリアランス値が30mL/min未満)のある患者[血中濃度が上昇し、副作用が発現するおそれがある。「用法・用量に関連する使用上の注意」「薬物動態」の項参照]
2)感染症の患者、感染症が疑われる又は再発性感染症の既往歴のある患者[感染症を悪化又は顕在化させるおそれがある。]
3)高齢者(「高齢者への投与」の項参照)
2. 重要な基本的注意
本剤の投与は尋常性乾癬及び関節症性乾癬治療に十分な知識・経験をもつ医師のもとで行うこと。
3. 相互作用
併用注意(併用に注意すること)

薬剤名等	臨床症状・措置方法	機序・危険因子
CYP3A4酵素誘導作用を有する薬剤 (リファンピシン、フェノバルビタール、カルバマゼピン、フェニトイン等)	リファンピシンとの併用投与で本剤のAUC及びC_{max}の減少が報告されているので、併用する場合には、効果の減弱に注意すること。	本剤はCYP3A4で代謝されるため、CYP3A4酵素誘導剤を併用した場合に、本剤の血漿中濃度が減少すると考えられる。

4. 副作用
国内臨床試験では、本剤の全投与期間中に、安全性評価症例241例中71例(29.5%)に副作用が認められた。報告された主な副作用は、下痢11例(4.6%)、腹部不快感9例(3.7%)、鼻咽頭炎8例(3.3%)、軟便6例(2.5%)、乾癬5例(2.1%)、悪心4例(1.7%)であった(承認時)。
外国臨床試験(30mg 1日2回投与群併合)では、本剤の全投与期間中に、安全性評価症例2357例中1046例(44.4%)に副作用が認められた。報告された主な副作用は、悪心310例(13.2%)、下痢296例(12.6%)、頭痛130例(5.5%)、緊張性頭痛64例(2.7%)、上気道感染64例(2.7%)、嘔吐61例(2.6%)、鼻咽頭炎56例(2.4%)、消化不良53例(2.2%)、上腹部痛46例(2.0%)であった(承認時)。
1)重大な副作用
(1)重篤な感染症(0.7%)[注1]:ウイルス、細菌、真菌等による重篤な感染症があらわれることがあるので、観察を十分に行い、感染症が疑われた場合には適切な処置を行うこと。
(2)重篤な過敏症(0.1%未満)[注1]:アナフィラキシー等の過敏症があらわれることがあるので、観察を十分に行い、異常が認められた場合には直ちに投与を中止し、適切な処置を行うこと。
(3)重度の下痢(頻度不明)[注2]:重度の下痢があらわれることがあるので、観察を十分に行い、異常が認められた場合には、投与を中止するなど適切な処置を行うこと。
注1)外国臨床試験(30mg 1日2回投与群併合)の試験成績
注2)市販後に報告された副作用については頻度不明とした。

【承認条件】
医薬品リスク管理計画を策定の上、適切に実施すること。

●その他の使用上の注意については、添付文書をご参照ください。

PDE4阻害剤
薬価基準収載
オテズラ®錠 10mg 20mg 30mg
Otezla® Tablets
アプレミラスト錠
劇薬 処方箋医薬品:注意ー医師等の処方箋により使用すること

製造販売元
セルジーン株式会社
〒100-7010 東京都千代田区丸の内二丁目7番2号

資料請求先 おくすり相談室
TEL 0120-786702 FAX 0120-786703 受付時間 9:00~18:00(土・日・祝日・弊社休日を除く)
セルジーン株式会社ホームページ http://www.celgene.co.jp

OTZ28A04
2018年9月作成

Novartis Pharma K.K.

新しい発想で医療に貢献します

ノバルティスのミッションは、より充実した、
すこやかな毎日のために、新しい発想で医療に貢献することです。
イノベーションを推進することで、
治療法が確立されていない疾患にも積極的に取り組み、
新薬をより多くの患者さんにお届けします。

NOVARTIS

ノバルティス ファーマ株式会社
http://www.novartis.co.jp/